The Journal of Immunology

P2Y6 Receptor Antagonist MRS2578 Inhibits Neutrophil Activation and Aggregated Neutrophil Extracellular Trap Formation Induced by Gout-Associated Monosodium Urate Crystals

Payel Sil, Craig P. Hayes, Barbara J. Reaves, Patrick Breen, Shannon Quinn, Jeremy Sokolove and Balázs Rada

J Immunol 2017; 198:428-442; Prepublished online 30 November 2016;
doi: 10.4049/jimmunol.1600766
http://www.jimmunol.org/content/198/1/428

The Journal of Immunology is published twice each month by
The American Association of Immunologists, Inc.,
9650 Rockville Pike, Bethesda, MD 20814-3994.

Print ISSN: 0022-1767 Online ISSN: 1550-6606.

P2Y6 Receptor Antagonist MRS2578 Inhibits Neutrophil Activation and Aggregated Neutrophil Extracellular Trap Formation Induced by Gout-Associated Monosodium Urate Crystals

Payel Sil,* Craig P. Hayes,* Barbara J. Reaves,* Patrick Breen,† Shannon Quinn,‡ Jeremy Sokolove,§,¶ and Balázs Rada*

Human neutrophils (polymorphonuclear leukocytes [PMNs]) generate inflammatory responses within the joints of gout patients upon encountering monosodium urate (MSU) crystals. Neutrophil extracellular traps (NETs) are found abundantly in the synovial fluid of gout patients. The detailed mechanism of MSU crystal–induced NET formation remains unknown. Our goal was to shed light on possible roles of purinergic signaling and neutrophil migration in mediating NET formation induced by MSU crystals. Interaction of human neutrophils with MSU crystals was evaluated by high-throughput live imaging using confocal microscopy. We quantitated NET levels in gout synovial fluid supernatants and detected enzymatically active neutrophil primary granule enzymes, myeloperoxidase, and human neutrophil elastase. Suramin and PPADS, general P2Y receptor blockers, and MRS2578, an inhibitor of the purinergic P2Y6 receptor, blocked NET formation triggered by MSU crystals. AR-C25118925XX (P2Y2 antagonist) did not inhibit MSU crystal–stimulated NET release. Live imaging of PMNs showed that MRS2578 represses neutrophil migration and blocked characteristic formation of MSU crystal–NET aggregates called aggregated NETs. Interestingly, the store-operated calcium entry channel inhibitor (SK&F96365) also reduced MSU crystal–induced NET release. Our results indicate that the P2Y6/store-operated calcium entry/IL-8 axis is involved in MSU crystal–induced aggregated NET formation, but MRS2578 could have additional effects affecting PMN migration. The work presented in the present study could lead to a better understanding of gouty joint inflammation and help improve the treatment and care of gout patients. ***The Journal of Immunology*****, 2017, 198: 428–442.**

Gout is an inflammatory disease of the joints caused by an innate immune response to monosodium urate (MSU) crystal deposition within the synovial space. Gout affects millions of patients globally (1). The prevalence of gout and its associated comorbidities (such as diabetes, kidney disease, and cardiovascular disorders) has increased during the past decade (2–4) and is expected to rise in the future (5). Crystal deposition triggers gout inflammation that is driven by the proinflammatory cytokine IL-1β and accumulation of polymorphonuclear leukocytes (PMNs) (6–12).

MSU microcrystals cause mechanical shear and tearing of the adjoining synovial tissues, (9, 11, 13) and this damage alerts leukocytes, which start infiltrating the site (14). Macrophages produce IL-1β in response to the MSU crystals by activating the NLRP3 inflammasome (7, 8). IL-1β is a proinflammatory cytokine (15–17). Upon activation by MSU crystals, PMNs produce reactive oxygen species, release granule proteins such as myeloperoxidase (MPO) and human neutrophil elastase (HNE), and form neutrophil extracellular traps (NETs) (6–8). MPO and HNE are packaged in PMNs in primary granules and can be released by degranulation or NET formation (2, 18–22). NET formation is an antimicrobial mechanism by which PMNs trap pathogens (18–20). Uncontrolled NET formation, however, has been associated with several diseases, including gout (6, 8). During NET formation, the PMN nucleus undergoes delobulation and decondensation (21). The nuclear membrane disassembles, granules disintegrate, and the cytoplasmic and nuclear contents fuse (22). Citrullination of histones H3 and H4 by peptidyl arginine deaminase 4 (PAD4) is an important step leading to nuclear decondensation (18–20, 23, 24).

Although PMNs represent the most abundant leukocytes during gout inflammation, reaching a concentration of 10^8/ml in the synovial fluid (SF) (6), their role in the complex pathogenesis of gout has been unclear. A recent study by Schauer et al. (6) shed light on the dual role of PMNs in gout. In addition to their proinflammatory role in initiating and mediating inflammation in gout, PMNs also play a proposed subsequent anti-inflammatory role in limiting acute flares (6). PMNs and MSU crystals accumulate to form high-density consolidated structures called aggregated NETs (aggNETs) that limit inflammation in gout (6, 25). AggNETs set the stage for gouty tophi formation, a characteristic white material that appears at the beginning of the

*Department of Infectious Diseases, College of Veterinary Medicine, University of Georgia, Athens, GA 30602; †Institute of Bioinformatics, University of Georgia, Athens, GA 30602; ‡Department of Computer Science, Franklin College of Arts and Sciences, University of Georgia, Athens, 30602 GA; §Stanford University School of Medicine, Stanford, CA 94305; and ¶Internal Medicine and Rheumatology, VA Palo Alto Health Care System, Palo Alto, CA 94034

ORCIDs: 0000-0002-3510-6281 (P.B.); 0000-0002-8916-6335 (S.Q.).

Received for publication May 2, 2016. Accepted for publication October 23, 2016.

This work was supported by a startup fund from the Office of the Vice President for Research, University of Georgia (to B.R.).

Address correspondence and reprint requests to Dr. Balázs Rada, University of Georgia, 501 D.W. Brooks Drive, Room 313, Athens, GA 30602. E-mail address: radab@uga.edu

The online version of this article contains supplemental material.

Abbreviations used in this article: aggNET, aggregated NET; CB, cytochalasin B; ER, endoplasmic reticulum; HNE, human neutrophil elastase; MCT, multiple comparison test; MPO, myeloperoxidase; MSU, monosodium urate; NET, neutrophil extracellular trap; OA, osteoarthritis; PAD4, peptidyl arginine deaminase 4; PMN, polymorphonuclear leukocyte; SF, synovial fluid; SOCE, store-operated calcium entry; TMB, 3,3′,5,5′-tetramethylbenzidine.

resolution phase of acute gout flares (6, 26). Although NET formation plays a unique role in the mechanism of gout inflammation, its cellular and molecular mechanisms are not well understood. At this point, the phagocytic NADPH oxidase and the RIPK1–RIPK3–MLKL signaling pathway have been implicated in MSU crystal–stimulated NET formation (6, 27).

NET formation is a cell death mechanism during which PMNs release several intracellular molecules. Uric acid is a by-product of purine metabolism that causes gout (2). The breakdown of purines results in the formation and accumulation of ectonucleotides such as ATP, UTP, or UDP that are recognized as danger signals by cells (28–32). Immune cells, including PMNs, macrophages, and T cells, respond to extracellular nucleotides via purinergic receptors (31, 32). Extracellular nucleotides and purinergic receptors are involved in various PMN functions such as migration, degranulation, and reactive oxygen species formation (33). Their role in NET release has not been investigated yet. Recent data show that MSU microcrystals signal through the purinergic P2Y6 receptor in THP1 macrophages and human keratinocytes (28). The P2Y6 receptor has high affinity for UDP and is involved in IL-8–mediated chemotaxis of leukocytes (30, 32, 34, 35). In inflammatory bowel disease, P2Y6 receptor activation causes stimulation of IL-8 expression in the intestinal epithelium, which leads to PMN recruitment (36). Previous studies show that MRS2578, a potent and specific P2Y6R antagonist, inhibits IL-8 and IL-6 release in PMNs stimulated by defensins (37–43). Thus, we hypothesized that the P2Y6 receptor is required for MSU crystal–induced NET formation in human PMNs.

We show in the present study that MRS2578 hinders MSU crystal–triggered PMN activation and NET formation. Understanding the processes involved in inhibition of NET formation via P2Y6R signaling can help advance current gout therapeutics.

Materials and Methods

Materials

Stock solutions of suramin [8,8′-(carbonylbis(imino-4,1-phenylenecarbonylimino-4,1-phenylenecarbonylimino))bis-1,3,5-naphthalenetrisulfonic acid] (P2Y inhibitor, 300 μM; Sigma-Aldrich, St. Louis, MO), MRS2578 (P2Y6 inhibitor, 5–10 μM; Sigma-Aldrich), PPADS (P2Y inhibitor, 200 μM; Tocris Bioscience, Minneapolis, MN), AR-C118925xx (P2Y2 antagonist, 1 μM; Tocris Bioscience), and a neutrophil elastase inhibitor [1-(3-methylbenzoyl)-1H-indazole-3-carbonitrile, $C_{16}H_{11}N_3O$; Cayman Chemical, Ann Arbor, MI) were prepared in DMSO. Sources for other reagents are as follows: saponin, cytochalasin B, ATP, ADP, adenosine, and UDP were purchased from Sigma-Aldrich. Additional reagents, their sources, and final doses used were SK&F96365 (store-operated calcium entry [SOCE] inhibitor, 100 μM; Tocris Bioscience), lucigenin (100 μg/ml; Cayman Chemical), human recombinant IL-8 (250 pg/ml, Cell Sciences, Canton, MA), anti-MPO Ab (Millipore, Billerica, MA), anti-HNE Ab (Calbiochem, Billerica, MA), Sytox Orange (Life Technologies, 2.5 μM; Invitrogen, Carlsbad, CA), 3,3′,5,5′-tetramethylbenzidine (TMB; Thermo Scientific, Waltham, MA), MSU crystals (InvivoGen, Carlsbad, CA), BSA (HyClone, GE Healthcare Life Sciences, Logan, UT), PBS (Thermo Scientific, Fremont, CA), and PMA (Sigma-Aldrich).

Human subjects

Healthy human volunteers were recruited anonymously at the University of Georgia to donate blood. The studies were performed according to the guidelines of the World Medical Association's Declaration of Helsinki. Enrolled blood donors signed consent forms with appropriate introduction as described previously (44, 45). The human blood protocol (University of Georgia protocol no. 2012-10769) and the consent form were reviewed and approved by the Institutional Review Board of the University of Georgia.

Preparation of human neutrophils and autologous serum

Human PMNs were purified as described previously (45). Briefly, coagulation was prevented with heparin and RBCs were removed by dextran sedimentation (GE Healthcare, Atlanta, GA). PMNs were isolated using Percoll (Sigma-Aldrich) gradient centrifugation. Cell viability was determined by trypan blue dye extrusion (>98%). PMN purity was assessed by cytospins and flow cytometry. The characterization confirmed >95% purity. Autologous serum was prepared by centrifugation and sterile filtration. Calcium- and magnesium-containing HBSS (Mediatech, Manassas, VA) supplemented with 1% autologous serum of the PMN donor, 5 mM glucose, and 10 mM HEPES was used as an assay buffer. Human PMNs were identified on the basis of the scattering pattern and also staining with CD16 and CD66abce-PE Abs (Miltenyi Biotec, San Diego, CA) using LSR II flow cytometer and BD FACSDiva v6 software.

SF samples

SF samples were acquired from patients diagnosed with gout or osteoarthritis (OA) under protocols that were approved by the Stanford University Institutional Review Board and included the informed consent of the subjects. Samples of SF from actively inflamed large or medium joints were obtained by needle aspiration performed by a board-certified rheumatologist at the VA Palo Alto Healthcare System or Stanford Hospital and Clinics (both in Palo Alto, CA). Grossly bloody fluid was excluded from analysis. SF was centrifuged at 1000 × *g* for 10 min, and supernatants were removed and frozen at −80°C until they were later used for the experiments described below. The diagnosis of gout was confirmed by identification of negatively birefringent intracellular needle-shaped MSU crystals on microscopic examination of SF under polarizing light microscopy. The diagnosis of OA was made as defined by the 1986 American College of Rheumatology (46).

Extracellular DNA release

NETs were quantified essentially as described (47, 48). Briefly, PMNs were allowed to adhere to poly-D-lysine–coated 96-well black transparent-bottom plates (Thermo Scientific, Rochester, NY) in assay buffer with 0.2% Sytox Orange (Life Technologies, Grand Island, NY). PMNs were then exposed to 250 μg/ml MSU crystals. Fluorescence (excitation, 530 nm; emission, 590 nm) was measured in a fluorescence microplate reader (Varioskan Ascent; Thermo Scientific) for 6 h at 37°C. Increase in fluorescence normalized on maximal value (saponin-treated PMNs) was referred to as extracellular DNA release and was expressed as percentage of maximum. Alternatively, results were also normalized against PMA.

Measurement of aggNET formation

One million PMNs resuspended in assay medium were seeded in a 48-well plate with or without 1 mg/ml MSU crystals at 37°C with 10 μM MRS2578 or 0.1% (v/v) DMSO. Images of aggNETs were taken after overnight incubation (6).

Quantification of enzymatic activities

To measure HNE activity, a neutrophil elastase activity assay kit (Cayman Chemical) was used following the manufacturer's protocol. Briefly, supernatants (50 μl) were placed into 96-well black plates. Substrate (Z-Ala-Ala-Ala-Ala 2Rh110, catalog no. 600613) solution was added to assess elastase activity by measuring production of the highly fluorescent product (compound R110) using 485-nm excitation and 525-nm emission wavelengths in a fluorescence plate reader (Varioskan Flash; Thermo Scientific). Data are expressed either as kinetics or endpoint values normalized on the maximal (PMA-stimulated) signal.

Peroxidase activity was measured by hydrogen peroxide–dependent oxidation of Amplex Red (Molecular Probes, Eugene, OR). Undiluted PMN supernatants (50 μl) were added to 96-well nontransparent black microplates (Costar, Corning, NY) and mixed with assay solution containing 100 μM Amplex Red and 100 μM hydrogen peroxide (Sigma-Aldrich). Production of the fluorescent product was measured with a fluorescence plate reader (Varioskan Ascent; Thermo Scientific) after 30 min at 560-nm excitation and 590-nm emission wavelengths. Known MPO concentrations (stock, 125 ng/ml MPO; R&D Systems, Minneapolis, MN) were used as the standard to determine peroxidase activities of unknown samples. Results are expressed as equivalent nanograms per milliliter MPO activity. This data presentation was preferred (instead of showing unit enzymatic activities per time and volume) to compare MPO concentration and activity in PMN supernatants.

Live imaging of NET formation using confocal microscopy

Human PMNs (2×10^6) in assay medium were incubated for 4 h at 37°C with or without 100 nM PMA or 100 μg/ml MSU crystals in 35-mm glass-bottom dishes (MatTek, Ashland, MA). The dishes were precoated for 1 h with 1% human serum albumin (Sigma-Aldrich) in HBSS. At the end of the incubation, 10 μM Sytox Orange (547–570 nm) (Invitrogen, Grand

Island, NY) was added prior to imaging. Images were collected using a Nikon A1R confocal microscope system equipped with the Perfect Focus System, high-speed motorization, and NIS-Elements software (Nikon Instruments, Melville, NY). Live cell imaging was carried out using a Tokai Hit INY-G2A-TIZ incubator (Tokai Hit, Shizuoka-ken, Japan) that controlled for temperature, humidity, and CO_2. The imaging was performed every 15 min for 16 h. The Coherent Sapphire 561-nm, 20-mW laser was used to excite Sytox Orange using a CFI Plan APO VC ×60 oil (numerical aperture, 1.4; working distance, 0.13 mm) objective. Z-stacks were acquired and three-dimensional image reconstructions were processed using the Nikon NIS-Elements version 4 software. Final image preparation was carried out using Adobe Photoshop.

High-throughput live imaging and quantitation of NET formation

PMNs were seeded at a concentration of 250,000 cells/well in a 96-well optical-bottom pit polymer base black plate (Thermo Scientific). PMNs were preincubated with 10 μM MRS2578 for 1 h prior to imaging. PMNs were then stimulated with 200 μg/ml MSU crystals for 16 h. A Nikon A1R confocal microscope system with a ×10 lens was used to capture transmitted light and fluorescence images. A field of interest was chosen to perform imaging, and image position was defined using the NIS-Elements software. The chosen field was a true representation of the entire well. Images were taken every 15 min for 12 h using the automated capture component of the NIS-Elements software. Mean Sytox Orange intensities of the fluorescent images were quantified using the "measure region of interest" feature of the software. The entire image that represented the field was selected as the region of interest. These measurements were used to calculate changes in Sytox Orange intensities over time (change in mean Sytox Orange intensity). Each biological replicate represents the mean of three technical replicates.

ELISA

Levels of MPO, HNE, and IL-8 were detected by ELISA. Manufacturer's instructions were followed for sample dilutions and processing. PMNs (250,000/well) were seeded in 96-well plates and stimulated with 250 μg/ml MSU crystals in HBSS for up to 4 h at 37°C. Cell supernatants collected were either immediately processed or stored (−20°C) for later analysis. Undiluted supernatants were used to measure IL-8 levels, whereas supernatants were diluted 1:100 to determine MPO and HNE concentrations. IL-8 release was measured by a human IL-8 ELISA kit (BioLegend, San Diego, CA). Concentrations of human MPO in PMN supernatants were measured by a commercial ELISA kit (R&D Systems). Serial dilutions prepared from the MPO standard provided in the kit (stock, 125 ng/ml) were used to quantify MPO concentrations of unknown samples. HNE release was assessed by sandwich ELISA using an anti-HNE rabbit polyclonal Ab to capture HNE. Supernatant samples were incubated overnight at 4°C in 96-well high-binding Microlon ELISA plates (Greiner Bio-One, Frickenhausen, Germany). After blocking with 5% BSA for 1 h, anti-rabbit mouse polyclonal Ab (1:500 in PBS, catalog no. 481001; EMD Millipore, Temecula, CA) was added for 2 h at room temperature. After repeated washes, samples were incubated with HRP-linked donkey anti-rabbit Ab (1:2000 in PBS, NA934V; GE Healthcare) for 1 h. Blue coloration developed in the presence of TMB (Thermo Scientific, Rockford, IL) peroxidase substrate solution. The reaction was stopped by adding 1 N hydrochloric acid, and absorption was read at 450-nm wavelength with an Eon microplate photometer (BioTek Instruments, Winooski, VT). Purified HNE standard (Cell Sciences) was used to determine HNE concentrations in unknown samples.

MPO-DNA and HNE-DNA ELISA assays

As described previously (44, 45), the concentration of HNE-associated DNA (definition for NETs) in PMN supernatants was measured using HNE capture Ab (1:2000, rabbit; Calbiochem), wheras MPO-associated DNA (NETs) was quantitated using MPO capture Ab (1:2000, rabbit; Upstate Biotechnology). Capture Abs were incubated overnight at 4°C. PMNs were treated with DNAse I (1 μg/ml; Roche) for 15 min at room temperature. DNAse digestion was stopped by adding 2.5 mM EGTA (Sigma-Aldrich). Supernatants were collected, centrifuged and diluted 10–100-fold in PBS+2.5 mM EGTA. For the NET standard, PMNs were incubated with PMA for 5 h. After 5 h, limited digestion of NETs was done for 10 min with 1 μg/ml DNase and the DNAse activity was stopped with 2.5 mM EGTA. A 2-fold serial dilution was made to generate the NET standard. High-binding 96-well ELISA microplates were blocked with 5% BSA/0.1% human serum albumin/PBS for 1–2 h followed by overnight incubation and three washes with Tween 20 in PBS. The diluted PMN supernatants were incubated overnight at 4°C. After 16 h of incubation, secondary anti–DNA-POD (HRP-conjugated anti-DNA Ab, mouse, 1:500; Roche) was added for 30–60 min at room temperature (44, 45). After three to four washes, TMB substrate was added. Absorbance was measured either at this point at 650 nm (kinetics) or after the addition of 1 M HCl stop solution at 450 nm (end point) with an Eon microplate spectrophotometer. Background absorbance values of the medium and untreated PMNs were subtracted.

NET immunofluorescence

PMNs (200,000) were seeded on sterile 12-mm round glass coverslips (VWR International, Radnor, PA) placed in 24-well plates (Thermo Scientific). MSU crystals (100 or 250 μg/ml) were added to PMNs and incubated for 4 h at 37°C. Coverslips were fixed with 4% paraformaldehyde (Affymetrix, Cleveland, OH) for 15 min. Cells were permeabilized and blocked with 5% BSA (VWR International), 5% normal donkey serum (Jackson ImmunoResearch Laboratories, West Grove, PA), and 0.1% Triton X-100 (Sigma-Aldrich) in PBS (Thermo-Scientific) for 30 min. PMNs were incubated with monoclonal rabbit anti-HNE Ab (1:250; Calbiochem, San Diego, CA) overnight at 4°C. After incubating with Alexa Fluor 594–labeled donkey anti-rabbit secondary Ab (1:500; Invitrogen, Eugene, OR) for 1 h, cells were stained with DAPI (2 min, room temperature, 1:20,000 of a 10 mg/ml stock solution; Molecular Probes, Grand Island, NY) and washed in PBS twice. Specimens were mounted using the ProLong antifade kit (Life Technologies) following the manufacturer's instructions and analyzed with Zeiss AxioCam HRm fluorescence microscope (Axioplan 2 imaging software).

Intracellular calcium signaling

To measure intracellular calcium mobilization from internal stores, PMNs were loaded with 2 μM Fluo-4 for 30 min in the dark in the presence of probenecid and pluronic acid in calcium-free HBSS. PMNs were washed twice with calcium-free HBSS and incubated with 10 μM MRS2578 or DMSO. PMNs were subsequently stimulated with 5 μg/ml ionomycin or 10 μM UDP in HBSS without calcium. Flow cytometer (LSR II flow cytometer) was used to monitor the calcium flux as described (49). The baseline reading was recorded for 1 min and then stimulation was added and immediate kinetics of the calcium flux were recorded for 3 min. The final analysis was performed using FlowJo software.

Phagocytosis assay

PMNs were seeded at a density of 2 million cells per dish with 50 μg/ml MSU crystals with 10 μM MRS2578 or 0.1% (v/v) DMSO (solvent control). Live videos were recorded for 1 h and MSU crystal-phagocytosing cells were counted at 30 and 60 min time points. At least 100 PMNs were counted as the total in each sample.

Superoxide production

PMNs (100,000/well) were seeded with 10 μM MRS2578 or 0.1% (v/v) DMSO (solvent control). PMNs were left either unstimulated or treated with 250 μg/ml MSU crystals or 100 nM PMA in the presence of 100 μg/ml lucigenin (superoxide-specific probe). Luminescence was measured for 60 min in a Varioskan Flash microplate luminometer. Integrated luminescence units (area under the curve) indicative of total superoxide production during the entire measurement were calculated and expressed as relative luminescence units.

Cell migration

Two million PMNs and 50 μg/ml MSU crystals were imaged for 1 h with or without 5 μM MRS2578. ImageJ Fiji software equipped with manual tracking and MTrackJ plugins was used to quantitate cell migration. PMNs were tracked every 2 s through 151 frames, and the videos were converted into grayscale. The average distance (micrometers) was measured for 9–13 PMNs per video for the final analysis. Optical flow was estimated for six pairs of videos. Videos consisted of 1024 × 1024 grayscale images with 60 frames per video. The Farneback method, implemented in OpenCV, was used to calculate dense optical flow between consecutive pairs of video frames. Flow vectors, containing horizontal and vertical displacement components, were computed at every pixel. The flow vectors were averaged to produce an aggregate delta x and delta y for each pair of video frames. This set of framewise delta x and delta y pairs was visualized using a two-dimensional contour plot. The algorithm has been deposited in an open-access online repository: https://github.com/quinngroup/JI-2016-MRS2578.

Statistical analysis

All data were statistically analyzed using GraphPad Prism software v6.01 (GraphPad Software, La Jolla, CA). A p value <0.05 was considered

significant. For multiple comparisons statistical analysis, a one-way ANOVA followed by a Dunnett multiple comparison test (MCT) test was used to compare each group with the control group. A Mann–Whitney *U* test was performed for nonparametric statistical analysis.

Results

NETs and neutrophil markers are present in gout SF

Although NETs and HNE have been previously detected in the gout synovial space (6–8), NETs and enzymatic activities of HNE and MPO have not been quantitated so far. To achieve this, we used ELISA assays established previously in our laboratory to detect NET-specific MPO-DNA and HNE-DNA complexes (45). OA is a degenerative joint disease with low-grade inflammation that is characterized by continual cartilage degradation (50, 51). SF from OA patients served as a suitable negative control for our experiment, because OA joint inflammation is not primarily driven by MSU crystals (46). Our analysis of 15 Gout and 11 OA SF supernatants obtained from consenting patients indicated the presence of larger quantities of MPO, DNA-associated MPO, HNE, and DNA-associated HNE in gout patient samples as compared with those taken from OA patients (Fig. 1A, 1C, 1D, 1F). Furthermore, we measured the presence of enzymatically active HNE and MPO enzymes and found significantly higher amounts in gout than in OA samples (Fig. 1B, 1E): MPO (629.9 ± 166.2 ng/ml, mean ± SEM, $n = 15$ [gout] and $n = 11$ [OA]), HNE (318.8 ± 38 ng/ml, mean ± SEM, $n = 15$ [gout] and $n = 11$ [OA]). Our conclusion is that NETs and enzymatically active PMN-derived enzymes are highly elevated in gout compared with OA.

MSU crystal phagocytosis is required for NET formation

Although the fact that PMNs attempt to phagocytose MSU crystals has been well documented, its requirement for NET formation remains unclear (52). To understand the link between crystal phagocytosis and NET release, a low concentration (50 μg/ml) of MSU crystals was used to enable clear visualization and recording of NET formations. As expected, PMNs tried to phagocytose MSU crystals under these conditions (Fig. 2A, 2B), as well. Live imaging during 12 h with the extracellular DNA-binding dye Sytox Orange showed that MSU crystals trigger DNA release in PMNs (Fig. 2C) in a crystal dose– and PMN concentration–dependent manner (data not shown). We performed image analysis to calculate the proportion of NET-forming PMNs among those associated with MSU crystals. Our analysis showed that PMNs that formed NETs represented 31.9 ± 2.3% (mean ± SEM, $n = 4$) of the total, crystal-associated pool whereas those not forming NETs were 68.1 ± 2.3% (mean ± SEM, $n = 4$) (Fig. 2D). Fig. 2E shows that 88.2 ± 13.7% (mean ± SEM, $n = 4$) of PMNs in contact with MSU crystals undergo NET formation, revealing that association with MSU crystals is required for NET release. The uptake of MSU crystals by PMNs depends on the cytoskeleton (53). To determine that the cytoskeleton is a critical component of MSU crystal–triggered NET release, we used cytochalasin B (CB), a known inhibitor of the actin cytoskeleton (47, 54). Fig. 2F shows that extracellular DNA release in response to MSU crystals is ablated in the presence of CB. As described by Schauer et al. (6, 25), high-density PMNs form aggNETs in the presence of

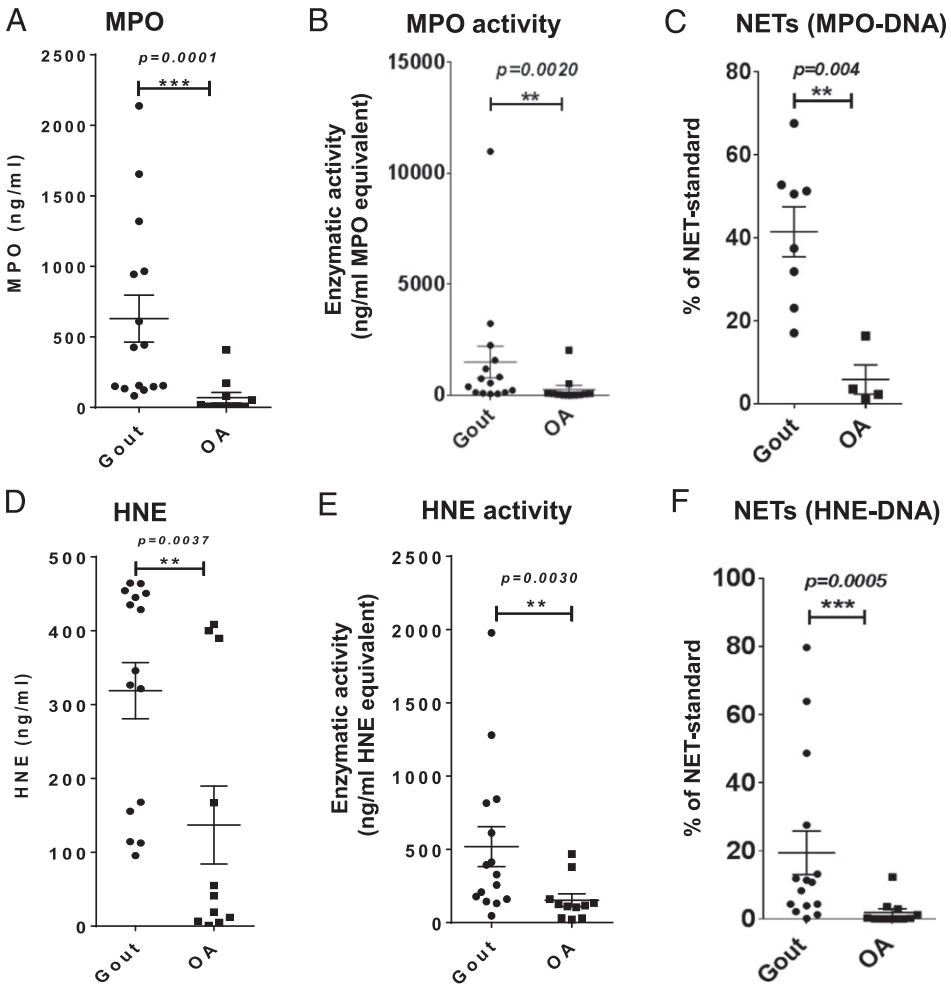

FIGURE 1. Gout SFs have elevated levels of NETs and enzymatically active MPO and HNE. MPO (**A**) and HNE (**D**) protein levels, their enzymatic activities (**B** and **E**), and NETs (**C** and **F**) were quantitated in SF supernatants of gout and OA patients. Protein levels were measured by commercial ELISA kits, enzymatic activities were assessed by fluorescent microplate assays, and MPO-DNA and HNE-DNA ELISAs were used to assess NET levels. In (A), (B), and (D)–(F), samples of 15 gout patients and 11 OA patients were compared. In (C), samples of eight gout and four OA samples were analyzed. Results are expressed as mean ± SEM. $*p < 0.05$, $**p < 0.01$, $***p < 0.001$. ns, not significant, Mann–Whitney *U* test.

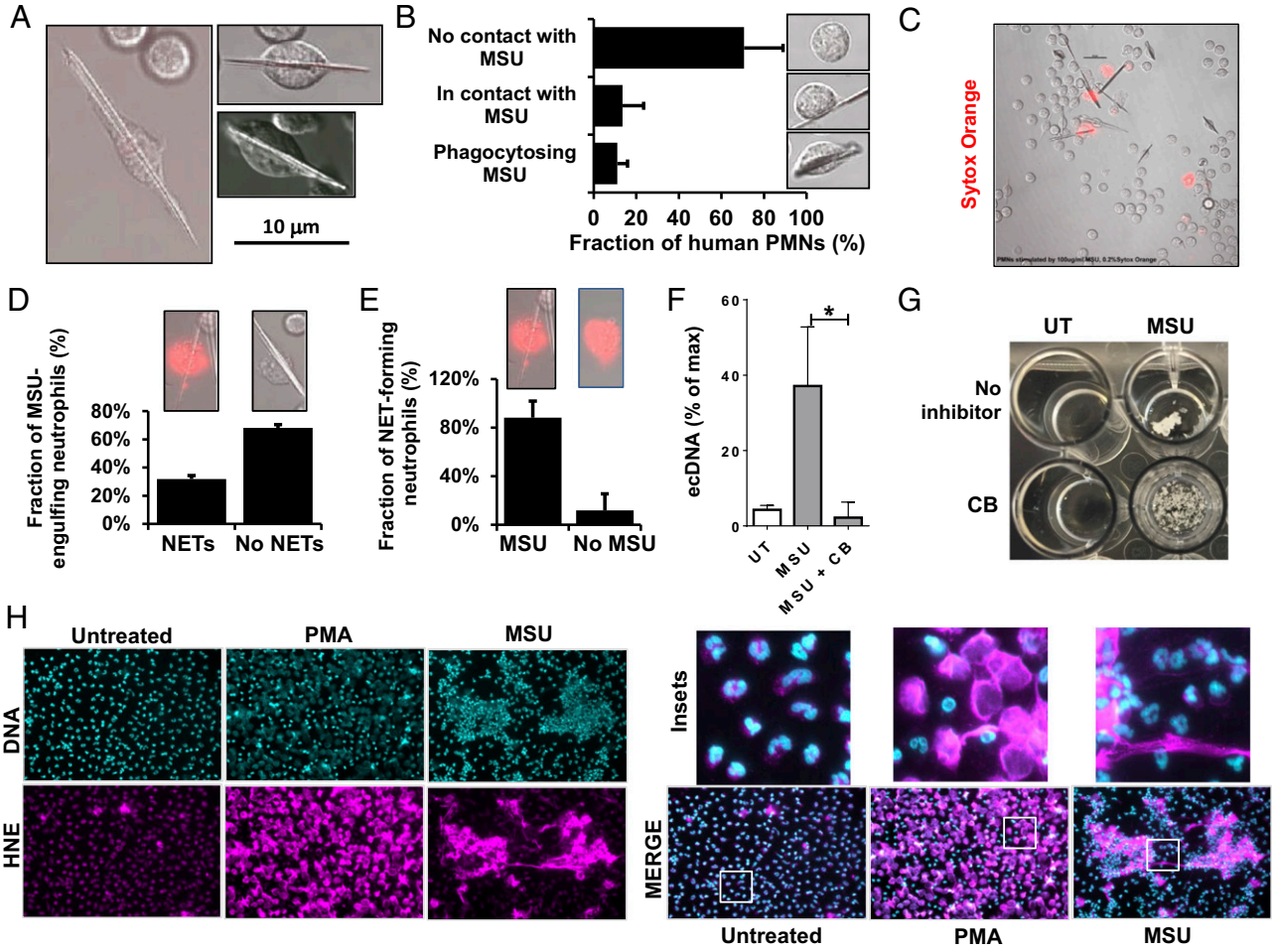

FIGURE 2. PMN cytoskeleton is requisite for MSU crystal-induced NET formation. (**A**) Human PMNs (250,000 cells/well) suspended in assay medium were incubated with 50 μg/ml MSU crystals for 3 h and differential interference contrast images of crystal-phagocytosing live cells were obtained by confocal microscopy (images of one representative experiment, $n = 5$). Scale bar, 10 μm. (**B**) Quantification of PMN–MSU crystal associations. Human PMNs incubated with MSU crystals (50 μg/ml, 3 h) were imaged with confocal microscopy. At least 50 PMNs/donor were categorized according to their association with MSU crystals (no contact; in contact with MSU crystal; phagocytosing MSU crystal). The percentage distribution of the three groups is presented as mean ± SEM of four independent PMN donors. Original magnification ×1500. (**C**) Human PMNs were incubated with 100 μg/ml MSU crystals for 3 h and stained with the fluorescent DNA-binding dye Sytox Orange. Images were recorded using a fluorescence microscope. One representative experiment of three similar ones is shown. Original magnification ×400. (**D**) Proportions of NET-forming PMNs and those without NET formation among MSU crystal-phagocytosing PMNs as total were calculated. Mean ± SEM, $n = 4$. Original magnification ×1500. (**E**) Proportions of MSU crystal–associated versus crystal-free cells among NET-forming PMNs were calculated. Mean ± SEM, $n = 4$. Original magnification ×1500. (**F**) Inhibition of MSU crystal phagocytosis by 10 μM CB blocks NET release (250 μg/ml MSU). NET formation was detected by Sytox Orange fluorescence. Mean ± SEM, $n = 3$. $*p < 0.05$, Dunnett MCT. (**G**) CB (10 μM) partially inhibits MSU crystal–induced aggNET formation. PMNs (2.5×10^6/well) in a 24-well plate were treated with CB and incubated overnight with 1 mg/ml MSU crystals. Representative images of three independent experiments are shown. (**H**) Immunofluorescence detection of MSU crystal–stimulated human PMNs reveals colocalization of HNE with extracellular DNA in NETs. Cells were left untreated or were activated by 250 μg/ml MSU crystals or 100 nM PMA for 3 h to generate NETs. PMNs were stained with primary anti-HNE Ab followed by treatment with secondary goat anti-rabbit Alexa Fluor 594 Ab. DNA was detected by DAPI. DAPI staining has been changed to light blue, whereas HNE staining is shown as cyan. Original magnification ×180. White boxes indicate insets shown magnified at the bottom of the figure. Original inset magnification ×1000. One representative result of four similar experiments received on four independent donors is shown. UT, untreated.

high doses of MSU crystals. In the synovium, these structures are thought to be precursors of gouty tophi (6, 25). Treatment of human PMNs in vitro with CB also delayed the formation of aggNETs (Fig. 2G). Thus, the cytoskeleton is required for complete MSU crystal–initiated NET and aggNET formation.

MSU-stimulated NETs bind HNE

HNE is a crucial NET marker previously shown to be present in NETs stimulated with either bacteria or PMA (20). To address whether HNE is a component of MSU crystal–triggered NETs, we performed immunofluorescence staining of crystal-exposed human PMNs. HNE staining in resting PMNs shows a typical granular pattern that does not overlap with the nuclear staining (Fig. 2H, insets). As expected, upon PMA stimulation most PMNs formed NETs and HNE colocalized with extracellular DNA (Fig. 2H). We also observed that 250 μg/ml MSU crystal–promoted NET release and HNE staining colocalized with the DNA staining in PMNs stimulated with the crystals for 4 h (Fig. 2H). These data confirm that PMNs stimulated with MSU crystals release NETs under our experimental conditions.

Purinergic P2Y receptors are involved in MSU crystal–triggered NET formation

NETosis is a form of cell death caused by various stimuli to cope with infection (18–20). MSU crystals are perceived as danger-associated molecules by PMNs (9). During PMN lysis, several

molecules, including nucleotides such as ATP, ADP, adenosine, UTP, and UDP, are released (31, 55). We hypothesized that extracellular nucleotides contribute to the signaling process of MSU crystal–initiated NET formation. Purinergic P2Y receptors represent a main class of receptors by which PMNs respond to extracellular nucleotides (28, 30, 31). Suramin and PPADS are widely used general inhibitors of P2Y receptors (56–60). Our data in Fig. 3A show that suramin inhibits the release of MPO-DNA complexes (NETs) in a dose-dependent manner. Suramin could not be tested in the Sytox Orange assay because it interfered with the fluorescent signal (data not shown). It has also been reported that suramin inhibits the enzymatic activity of HNE (61, 62). Data presented in Fig. 3B show that suramin exhibited a partial inhibitory effect on HNE activity in concentrations previously used in PMNs in our hands, as well. The involvement of HNE in the signaling driving NET formation is still under investigation. Although initial studies indicated its involvement in NET release (63, 64), recent data show that HNE is dispensable for NET formation under certain conditions (65). To assess whether HNE is required for MSU crystal–induced NET release in human PMNs, we used 1-(3-methylbenzoyl)-1H-indazole-3-carbonitrile, a potent, competitive, and pseudoirreversible HNE inhibitor (66). This inhibitor strongly inhibited HNE activity in a cell-free system (Fig. 3C). The same HNE inhibitor, however, failed to inhibit MSU crystal–stimulated ecDNA release in human PMNs in the same concentration range (Fig. 3D). Thus, although suramin interferes with HNE activity in our experimental system, HNE is not required for NET release by MSU crystals, so suramin's inhibition of HNE cannot be responsible for suramin's block of MSU crystal–induced NET release. Other mechanisms, likely through purinergic receptors, must account for it. To confirm this, we used another general purinergic receptor inhibitor, PPADS, and tested its effect on NET release. As shown in Fig. 3E, PPADS led to partial inhibition of MSU crystal–triggered NET release, indicating the involvement of purinergic receptors in the process. Among purinergic receptors, P2Y2 has been shown to be the main receptor expressed in PMNs (55, 67–69). ARC118925XX, a specific P2Y2 antagonist, did not inhibit MSU crystal–induced NET release (Fig. 3F). Thus, purinergic receptors other than P2Y2 must drive NET release triggered by MSU crystals.

P2Y6R inhibitor MRS2578 blocks MSU crystal–induced NET formation

Several members of the P2YR family are expressed in human PMNs (28, 70). P2Y6R has been shown to be involved in cytokine release in PMNs (28). P2Y6R biology can be studied using a highly specific inhibitor, MRS2578 (71). MRS2578 fully inhibits P2Y6R in the lower micromoles per liter concentration range (28, 32, 37, 42, 71–73). We

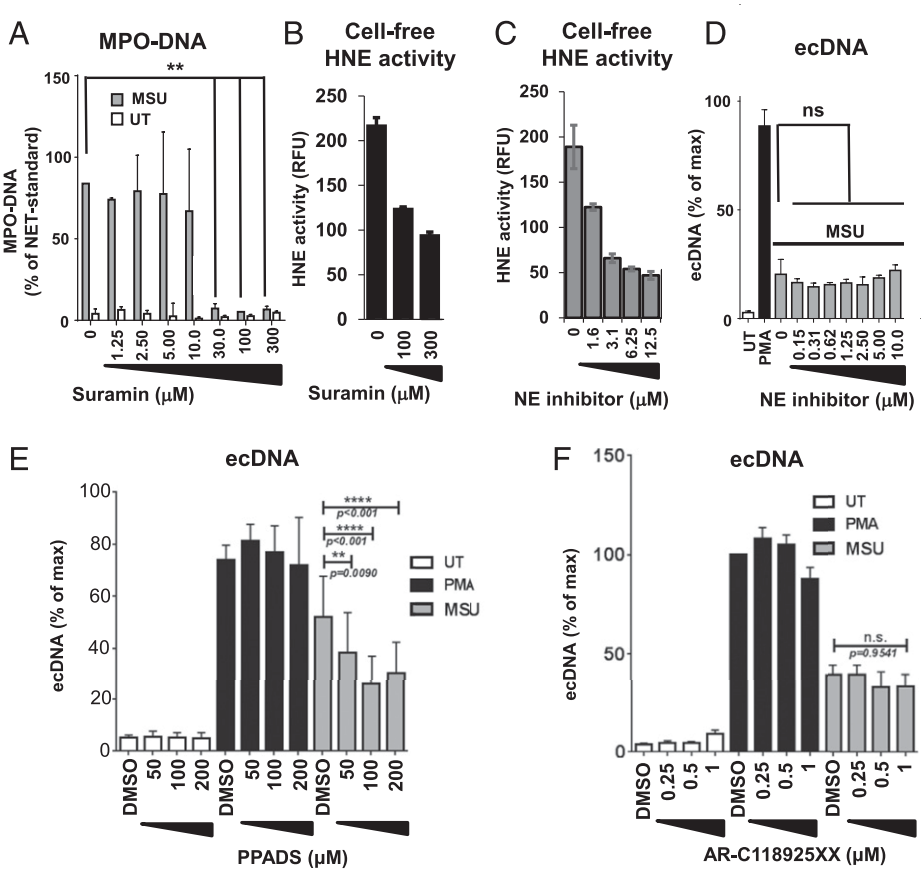

FIGURE 3. General inhibitors of purinergic receptors inhibit MSU crystal–initiated NET release. (**A**) Human PMNs were stimulated with 250 μg/ml MSU crystals, and NET formation was measured by MPO-DNA ELISA in the presence of increasing doses of the P2YR inhibitor suramin ($n = 3$, mean ± SEM, Dunnett MCT). (**B**) HNE enzymatic activity was measured in a cell-free system in the presence of suramin using a commercial kit (mean ± SEM, $n = 3$). (**C**) Cell-fee HNE activity was measured as described in the presence of a neutrophil elastase–specific inhibitor (mean ± SEM, $n = 3$). (**D**) Extracellular DNA release was measured in MSU crystal–stimulated human PMNs using Sytox Orange in the presence of indicated concentrations of the neutrophil elastase inhibitor (mean ± SEM, $n = 3$). (**E**) MSU crystal–stimulated extracellular DNA release is inhibited by the general purinergic receptor inhibitor PPADS (Sytox Orange, mean ± SEM, $n = 4$). (**F**) Blocking P2Y2 by its specific inhibitor, ARC118925XX, in human PMNs has no effect on extracellular DNA release induced by MSU crystals (Sytox Orange, $n = 3$, mean ± SEM). *$p < 0.05$, **$p < 0.01$, ***$p < 0.001$. ecDNA, extracellular DNA; NE, neutrophil elastase; ns, not significant; UT, untreated.

assessed whether MRS2578 inhibits NET formation. As the data presented in Fig. 4 show, MRS2578 blocked MSU crystal–induced releases of DNA, MPO, HNE, and HNE-DNA complexes from human PMNs. Trypan blue staining of PMNs confirmed that MRS2578 is not toxic to PMNs (data not shown). This observation indicates the novel involvement of the purinergic P2Y6 receptor in MSU crystal–induced NET release.

Extracellular nucleotides alone fail to initiate NET formation

The main ligand of P2Y6R is UDP, but it also binds UTP with lower affinity (70, 74). P2Y6R does not respond to adenine-based nucleotides (70, 74). UDP and UTP are released from damaged cells and are reported to stimulate PMNs via P2Y6R (75–78). ATP, ADP, and adenosine increase migration and IL-8 release in PMNs (31, 37, 74). Therefore, we asked whether NET formation could be initiated in human PMNs by stimulating them with micromolar or lower millimolar concentrations of adenine- and uridine-based nucleotides. As the results in Fig. 5 show, ATP, ADP, adenosine, UTP, or UDP did not induce NET release in human PMNs when stimulated with concentrations up to the lower millimoles per liter concentration range. On the contrary, ATP had a slight inhibitory effect at higher doses (Fig. 5A). Tested ectonucleotides were also without any significant effect on MSU crystal– or PMA-induced NET release (Fig. 5C–E). These data indicate that P2Y6R does not directly trigger NET formation in PMNs.

P2Y6R inhibition blocks aggNET formation

As described by Schauer et al. (6, 25), high-density cultures of PMNs form aggNETs that help in resolving joint inflammation. In the synovium, these structures are precursors of gouty tophi (6, 25). To test the effect of MRS2578 on aggNET formation, we incubated high-density cultures of PMNs and MSU crystals in vitro with or without 10 μM MRS2578 or 0.1% DMSO (vehicle control). AggNETs formed after overnight incubation (Fig. 6C). To better understand the complex mechanism of MSU crystal–induced aggNET formation, we established a high-throughput method capable of imaging NET formation during long periods of time in several samples in parallel. This high-throughput live-imaging method using 96-well microplates and automated confocal microscopy confirmed that human PMNs release NETs in response to MSU crystals and PMA, as well (Fig. 6A). Similarly to our previous data, MRS2578 inhibited the NET-forming ability of MSU crystals under these conditions, as well (Fig. 6A, 6B). Interestingly, NET formation triggered by PMA was also delayed by MRS2578 (Fig. 6B). The recorded series of images revealed a migratory component of aggNET formation specific for MSU crystal stimulation (Fig. 6A). First, small, early microaggregates appeared in the first few hours that merged later into large, macroscopic aggNETs (Fig. 6B, 6C). PMNs without stimulation or in the presence of PMA failed to show this phenotype (Fig. 6A). MRS2578 had a complete inhibitory effect on MSU crystal–induced aggNET formation (Fig. 6C, images at 5 h) and also on this proposed migratory component, indicating that the inhibitor prevents MSU crystal–induced NET formation by blocking PMN movement.

MRS2578 inhibits MSU crystal–induced IL-8 release

Because UDP also stimulates IL-8 release in PMNs (31, 33, 55, 74), we investigated the effect of MRS2578 on MSU crystal–induced release of IL-8 as our primary candidate mediating PMN migration. IL-8 signaling causes adhesion, degranulation, respiratory burst, and lipid mediator synthesis in PMNs (79). TNF-α–primed PMNs stimulated with IL-8 are able to produce NETs (80). In Fig. 7A, we show that MSU crystal–induced IL-8 secretion is

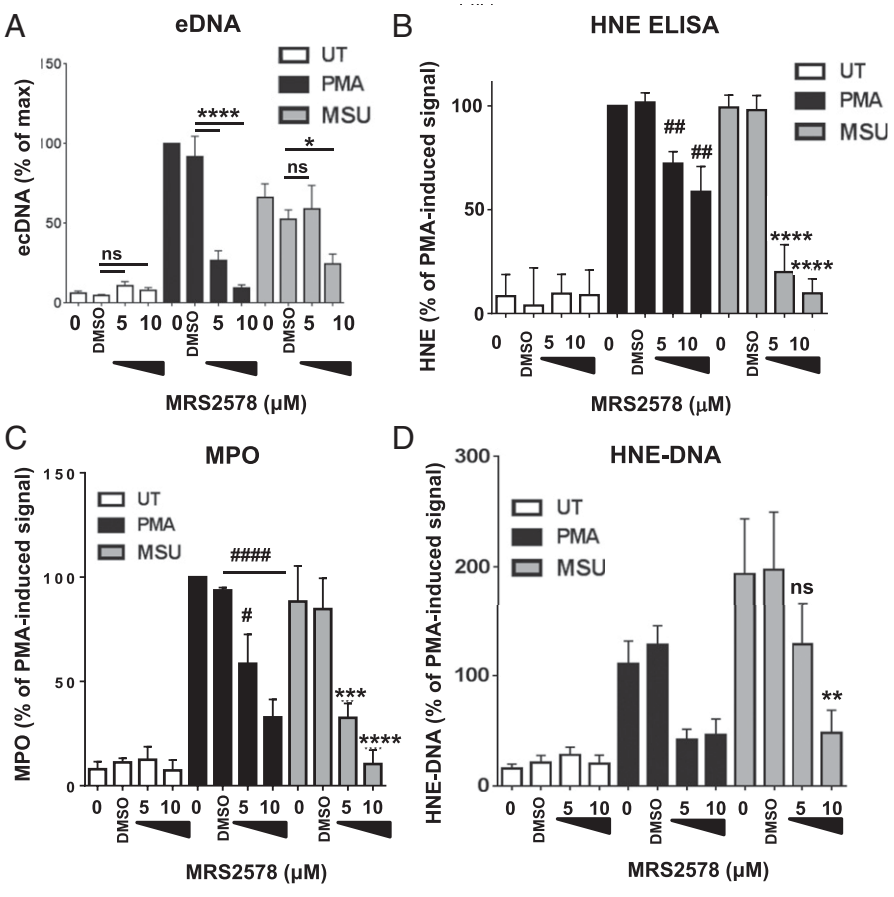

FIGURE 4. The P2Y6 receptor antagonist MRS2578 inhibits NET release induced by MSU crystals and PMA. Human PMNs were treated with 5 or 10 μM MRS2578 for 1 h prior to stimulation with 250 μg/ml MSU crystals or 100 nM PMA to trigger NET release. Endpoint measurements of (**A**) Extracellular DNA (ecDNA) release (4 h, $n = 3$, mean ± SEM), (**B**) HNE release (ELISA, 4 h, $n = 3$, mean ± SEM), (**C**) MPO release (ELISA, 4 h, $n = 5$, mean ± SEM), and (**D**) NET release (HNE-DNA ELISA, 4 h, $n = 5$, mean ± SEM) were measured. Data are shown as mean ± SEM. Nonparametric statistical analysis (Dunnett MCT) was used to establish significance. $^{*}p < 0.05$, $^{***}p < 0.001$, $^{\#\#}p < 0.01$, $^{\#\#\#\#}p < 0.0001$. ns, not significant; UT, untreated.

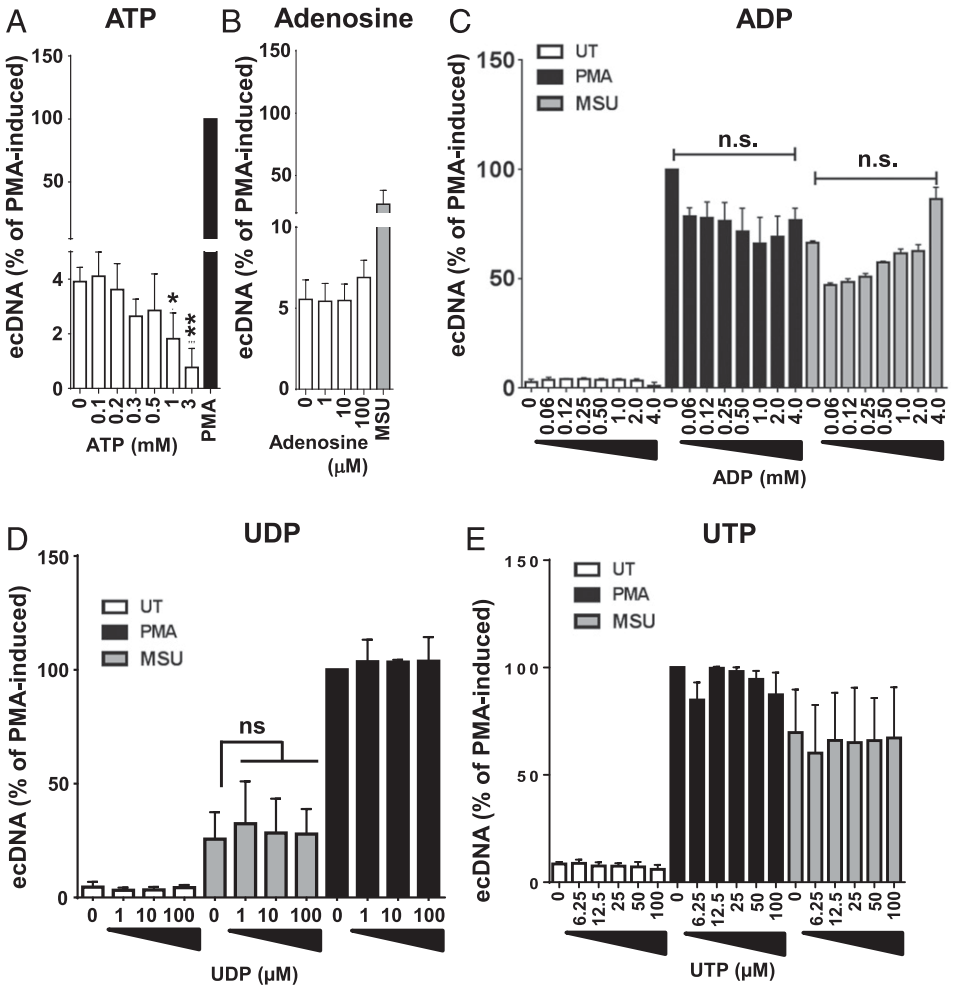

FIGURE 5. Ectonucleotides do not trigger NET release. Human PMNs were left unstimulated or stimulated with 100 nM PMA or 250 μg/ml MSU crystals in the presence of different doses of (**A**) ATP ($n = 4$), (**B**) ADP ($n = 3$), (**C**) adenosine ($n = 3$), (**D**) UDP ($n = 3$), and (**E**) UTP ($n = 3$). Extracellular DNA (ecDNA) release was measured by Sytox Orange–based fluorescence and normalized to the signal obtained by PMA without ectonucleotides. Statistical significance was established by Dunnett MCT. Mean ± SEM, n = at least 3. $*p < 0.05$, $***p < 0.001$. ns, not significant; UT, unstimulated (no MSU or PMA).

inhibited by MRS2578, which is in agreement with similar results of other groups using different stimuli (28, 37, 42).

MRS2578 prevents phagocytosis of MSU crystals by PMNs

Because PMNs have been shown to phagocytose MSU crystals, a step that is required for NET release (see Fig. 2), we next tested whether P2Y6 inhibition affects crystal phagocytosis. Low-density cultures of human PMNs were exposed to MSU crystals, and crystal-phagocytosing PMNs were quantitated using microscopy. As shown in Fig. 7B, MRS2578 significantly inhibited the ability of PMNs to phagocytose MSU crystals.

MRS2578 blocks the PMN respiratory burst

The NADPH oxidase expressed in PMNs produces reactive oxygen species that are required for efficient intracellular bacterial killing and also NET formation induced by several stimuli (21, 23, 81, 82). MSU crystal–induced NET formation has been reported to be NADPH oxidase–dependent (6). To learn whether MRS2578 inhibits NET formation up- or downstream of the NADPH oxidase, we exposed human PMNs to MSU crystals after treatment with the inhibitor. MRS2578 exposure led to a complete block of both spontaneous and crystal-initiated superoxide production (Fig. 7C). This finding suggests that P2Y6R is located upstream of the NADPH oxidase.

Reduction of UDP-stimulated calcium flux by MRS2578

G protein–coupled receptors such as P2Y6R activate phospholipase C, and UDP causes a steep rise in intracellular calcium concentration by releasing calcium from intracellular stores (83). In PMNs, calcium is required for phagolysosome fusion, chemotaxis, release of proteins from granules, and changes in cytoskeleton (36, 42, 78, 84–87). In Fig. 7D we observed that inhibition of P2Y6R resulted in inhibition of UDP-stimulated calcium release from the intracellular stores (in Ca^{2+}-free medium). This indicates that PMNs express a functional P2Y6R, and MRS2578 strongly interferes with this signal.

MRS2578 inhibits spontaneous migration of PMNs

Our previous data (Fig. 6A) indicated that an active migratory component is involved in MSU crystal–induced aggNET formation that could be the target of MRS2578's inhibitory action. AggNET-forming PMNs stimulated with MSU crystals create a very complex system in which individual cell migration is difficult to study. Therefore, we exposed a low-density culture of PMNs to MSU crystals and followed their migration with time-lapse microscopy with the purpose to assess whether MRS2578 affects their inherent migratory ability. Human PMNs performed random migration over time when left untreated (Fig. 8A, Supplementa1 Video 1). Addition of MRS2578 resulted in an inhibition of PMN migration by 82.5 ± 5.4% on average (Fig. 8, Supplemental Video 2). These results indicate that MRS2578 primarily affects the migratory/chemotactic component of MSU crystal–induced aggNET formation.

Blocking the SOCE pathway partially inhibits NET formation

The main route of calcium mobilization during PMN activation is the SOCE mechanism (88, 89). The role of SOCE in NET formation has not been explored yet. In the present study, we show

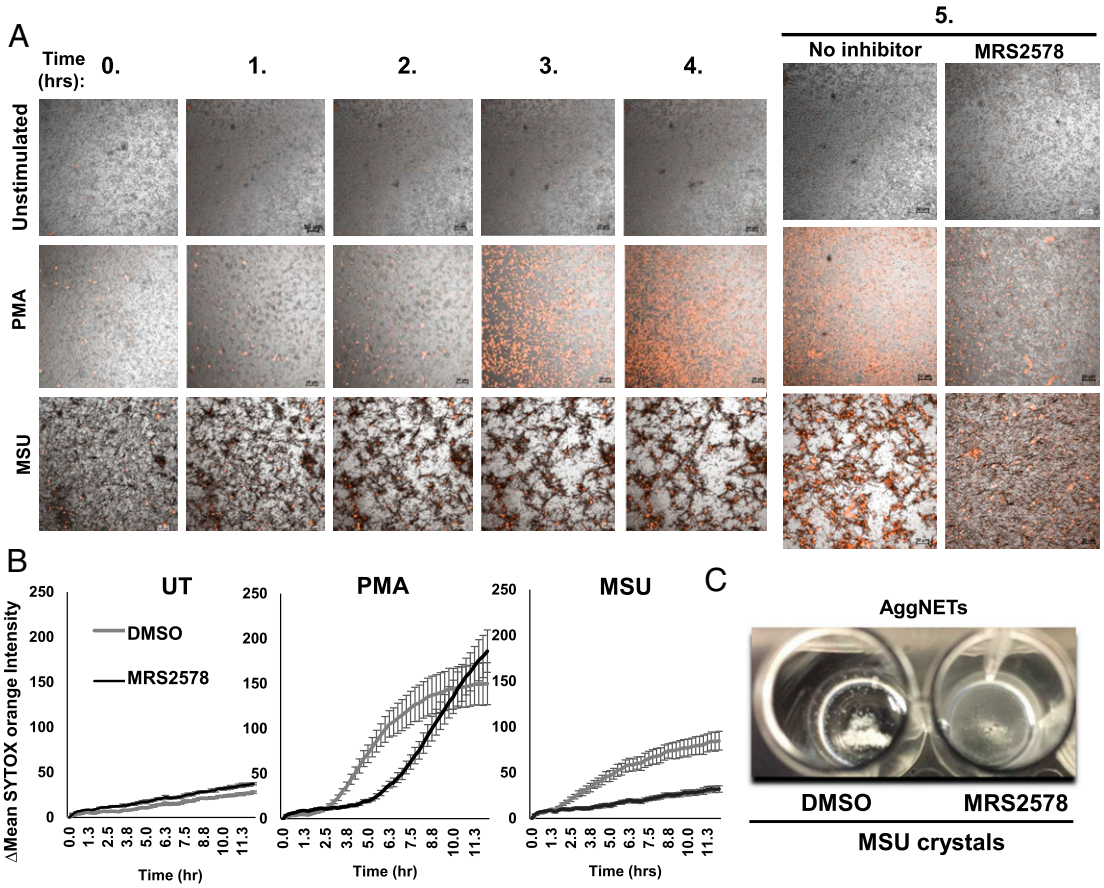

FIGURE 6. MRS2578 blocks MSU crystal–induced aggNET formation. (**A**) PMNs (250,000) were incubated in wells of 96-well microplates with or without MRS2578 (10 μM) for 1 h prior to stimulation with 250 μg/ml MSU crystals or 100 nM PMA for 5 h in the presence of the extracellular DNA-binding dye Sytox Orange. Interactions of PMNs and MSU crystals were monitored using confocal microscopy equipped with a motorized and heated stage support every 15 min (n = 3). Original magnification for images at 0–4 h, ×100; original magnification for images at 5 h, ×120. (**B**) Representative kinetics of the same experiments are shown (n = 3, mean ± SD). (**C**) One million PMNs were stimulated with 1 mg/ml MSU crystals in 24-well plates in the presence or absence of 10 μM MRS2578 or 0.1% DMSO (vehicle control). Formed aggNETs were recorded after overnight incubation (one representative image, n = 3).

hat the SOCE inhibitor SK&F96365 partially inhibits MSU crystal–induced NET release (Fig. 9A). Releases of MPO and HNE initiated by MSU crystals were also significantly reduced by this inhibitor (Fig. 9B, 9C). PMA-induced NET formation was not affected by SK&F96365 (Fig. 9A–C). SK&F96365 also blocked MSU crystal–triggered IL-8 release (Fig. 9D). These data suggest that SOCE specifically promotes MSU crystal–induced NET formation in human PMNs.

Discussion

The present study demonstrates that elevated levels of NETs and NET-associated markers, including active MPO and HNE, are present in SF supernatants of gout patients. Although NETs have previously been detected in the SF of gout patients (6, 7), our NET-specific ELISA assays (44) quantitate NETs, to our knowledge for the first time, in clinical biospecimens of gout patients. We have previously only used the HNE-DNA ELISA on live human PMNs (44). To our knowledge, results presented in the current study are the first to show its use for NET quantitation in clinical samples of any human disease. Both the MPO-DNA and HNE-DNA ELISA assays have great promises as NET-specific quantitation tools (44, 48). Our data also detect enzymatically active MPO and HNE, two primary granule markers released by PMNs, indicating that both enzymes remain active in gout SF, potentially contributing to joint damage. HNE could contribute to disease pathogenesis via several mechanisms. Once released, HNE degrades almost each component of the extracellular matrix (90, 91). In the lung, HNE can cause direct damage in epithelial cells and can impair mucociliary clearance and increase mucus secretion (92–94). HNE is considered the main factor damaging lungs of cystic fibrosis, chronic obstructive pulmonary disease, and emphysema patients (95–97). Free-floating HNE could potentially cause similar pathologic effects in the SF of gout patients, including directly damaging synoviocytes and activating PMNs/macrophages. Alternatively, HNE also degrades proinflammatory cytokines, thereby limiting the breadth/extent of gout flares (6). Addressing a potential, clinically relevant correlation of gout SF or blood levels of NETs and granule enzyme activities with gout disease severity is hindered by the difficulty of adequate clinical scoring of relative joint inflammation in gout (98–100).

The quantitative analysis using live imaging of crystal–PMN interactions revealed that almost all PMNs releasing NETs were associated with MSU crystals. This suggests that physical interaction between PMNs and crystals is required to trigger NET formation. This finding conflicts with a previous study stating that crystal phagocytosis is not a requirement for NET generation (101). Our data using CB show that an active cytoskeleton is required for NET release. We have also reported the requirement of an intact cytoskeleton for NET formation stimulated by pseudogout-associated calcium pyrophosphate dihydrate crystals (47) and *Pseudomonas aeruginosa* (45). This indicates that an intact phagocytic apparatus is required to trigger NETs induced by particulate stimuli.

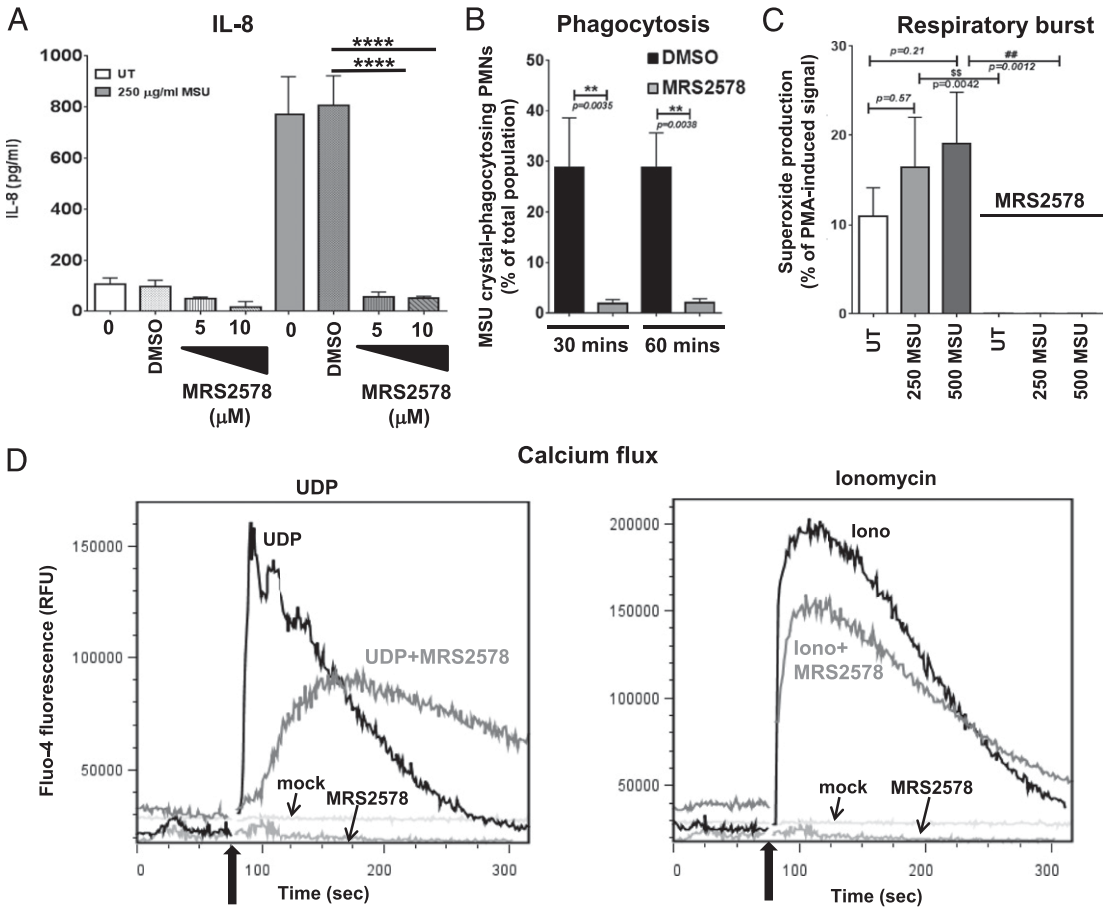

FIGURE 7. MRS2578 inhibits MSU crystal–stimulated IL-8 release, superoxide production and phagocytosis, and UDP-stimulated calcium flux in human PMNs. (**A**) PMNs were treated with the indicated concentrations of MRS2578 or 0.1% (v/v) DMSO for 1 h prior to stimulation with 250 μg/ml MSU crystals for 4 h. IL-8 levels were quantified in the supernatants using ELISA. Results are expressed as mean ± SEM ($n = 5$). ****$p < 0.0001$, Dunnett MCT. (**B**) Two million PMNs were treated with the indicated concentrations of MRS2578 or DMSO for 1 h. MSU (50 μg/ml) crystals were added prior to imaging and PMNs engulfing crystals were counted ($n = 4$, mean ± SEM). (**C**) PMNs were treated with the indicated concentrations of MRS2578 or DMSO for 1 h prior to stimulation with 250 or 500 μg/ml MSU crystals. Superoxide release was detected by a lucigenin-based chemiluminescence assay for 1 h. Results are expressed as mean ± SEM ($n = 3$). $^{\#\#}p < 0.001$, $^{\$\$}p < 0.001$, Dunnett MCT. (**D**) PMNs loaded with the calcium indicator Fluo-4 were incubated with MRS2578 or DMSO in calcium-free HBSS and subsequently stimulated with 5 μg/ml ionomycin or 10 μM UDP. Using flow cytometry, fluorescent intensity was measured and kinetics of the calcium flux were recorded during 300 s in calcium-free medium. Stimulation was added after the baseline reading was taken for 1 min. The kinetics are a representation of four independent experiments using PMNs obtained from independent donors each time. Black arrows indicate the addition of stimuli (ionomycin and UDP).

The mechanistic details of how MSU crystals induce NET formation remain to be studied. One possible mechanism is that crystals form pores in the PMN plasma membrane, leading to ion fluxes and initiation of NET release, similar to the activation of the NLRP3 inflammasome (102). Recently, it has been shown that soluble uric acid triggers NET formation (103). We do not think this mechanism plays a significant role in our system because transferring crystal-free supernatants of MSU crystal suspensions containing free MSU did not induce NET formation in human PMNs previously not exposed to crystals (data not shown). Alternative mechanisms suggested the involvement of specific surface receptors in MSU crystal–induced activation of PMNs (14, 53). We identified P2Y6R in the process, but future studies will address whether P2Y6R could directly bind to MSU crystals. The P2Y6 receptor could promote crystal phagocytosis because it has been shown to mediate phagocytosis in microglia cells stimulated with UDP (43, 77).

Similar to several cell death pathways, NET formation is also likely accompanied by release of copious amount of ectonucleotides such as ATP, ADP, UDP, UTP, and adenosine (104). These nucleotides bind to various purinergic receptors and regulate immune signaling (70). Purinergic signaling has been implicated as a fundamental element in several PMN functions, including migration, superoxide production, and various signaling pathways (55). One of their main functions is to direct PMN chemotaxis to sites of cell damage via P2Y purinergic receptors (70). Our data showing that purinergic receptor inhibitors suramin, PPADS, and MRS2578 block the action of MSU crystals are, to our knowledge, the first to indicate their involvement in NET formation. The involvement of P2YR signaling in the mechanism of NET formation raises several questions. Interestingly, nucleotides alone do not trigger NET formation. Suramin and PPADS are general P2YR antagonists (57, 58, 69, 105, 106). The P2Y2-specific antagonist ARC118925XX did not have any influence on MSU crystal–induced NETs. MRS2578 is highly specific for P2Y6R, which was confirmed in several studies using genetic (knockdown or overexpression) approaches (28, 70, 107, 108). MRS2578 does not affect P2Y2R because it impaired chemotaxis in P2Y2R knockout murine PMNs to the same extent as in wild-type, P2Y2-expressing PMNs (108). PMNs express several P2YRs, including P2Y6 (70, 108). The role of P2Y6 in PMN biology is not well understood. It is required for IL-8 release induced by UDP (70) and by MSU (our

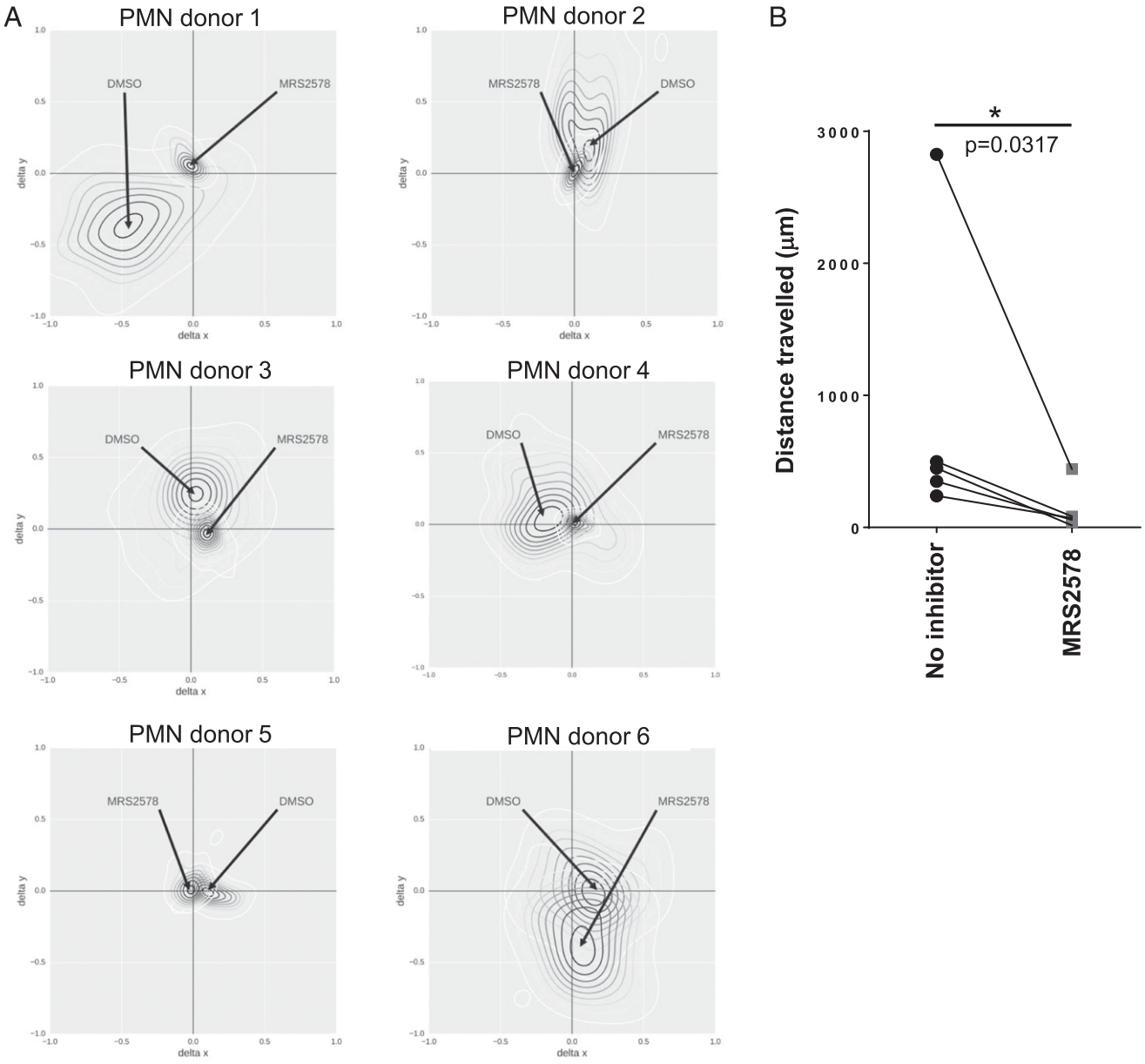

FIGURE 8. MRS2578 inhibits intrinsic migration of human PMNs. Human PMNs were pretreated with 10 μM MRS2578 or 0.1% DMSO for 1 h and their migration was recorded using a confocal microscope. PMNs obtained from six independent healthy donors were used. At least 10 individual PMNs per video were tracked. (**A**) The aggregate PMN displacement for each video was characterized by computing dense optical flow vectors over pairs of consecutive frames as described in *Materials and Methods*. Results are visualized as two-dimensional contour plots. (**B**) Total distances of migration per PMN were calculated using ImageJ software. Each pair of dots indicated by connectors represent individual donors. Results are expressed as mean ± SEM. $*p < 0.05$, Student t test.

data). P2Y6R could potentially mediate aggNET formation by regulating IL-8–mediated PMN migration (70). This is also likely because the ectonucleotidase NTPDase1 (CD39) has been shown to control IL-8 release in human PMNs (108). P2Y6R could also play a role because IL-8 release in epithelial cells induced by neutrophil defensins is blocked by MRS2578 (109). MRS2578 could also switch off NETosis in human PMNs, only to shorten their lifespan and accelerate apoptosis (72).

Some of the inhibitory results of MRS2578 are difficult to explain solely by its direct block of P2Y6R signaling. MRS2578 inhibited not only MSU crystal–induced NET release but also that triggered by PMA (Fig. 4). It is very unlikely that PMA signals via P2Y6R to release NETs. We think a more feasible explanation is that MRS2578 has off-target effects in addition to inhibiting P2Y6R signaling. The NADPH oxidase is our primary candidate as the nonspecific target of MRS2578 because spontaneous and MSU crystal–induced superoxide productions are both entirely blocked by the compound. An inhibition of the NADPH oxidase by MRS2578 would explain its inhibitory action on the respiratory burst and on several of the PMA-elicited PMN responses. MRS2578 is an isothiocyanate derivative, so it could potentially interfere with redox reactions such as superoxide production in PMNs. Previous data obtained with MRS2578 in PMNs should also be reevaluated and more carefully interpreted. Experiments using murine PMNs deficient in different purinergic receptors would help to determine the exact mechanism of action of MRS2578 in PMNs. The results presented in the present study showing that MRS2578 inhibits PMN migration, reactive oxygen

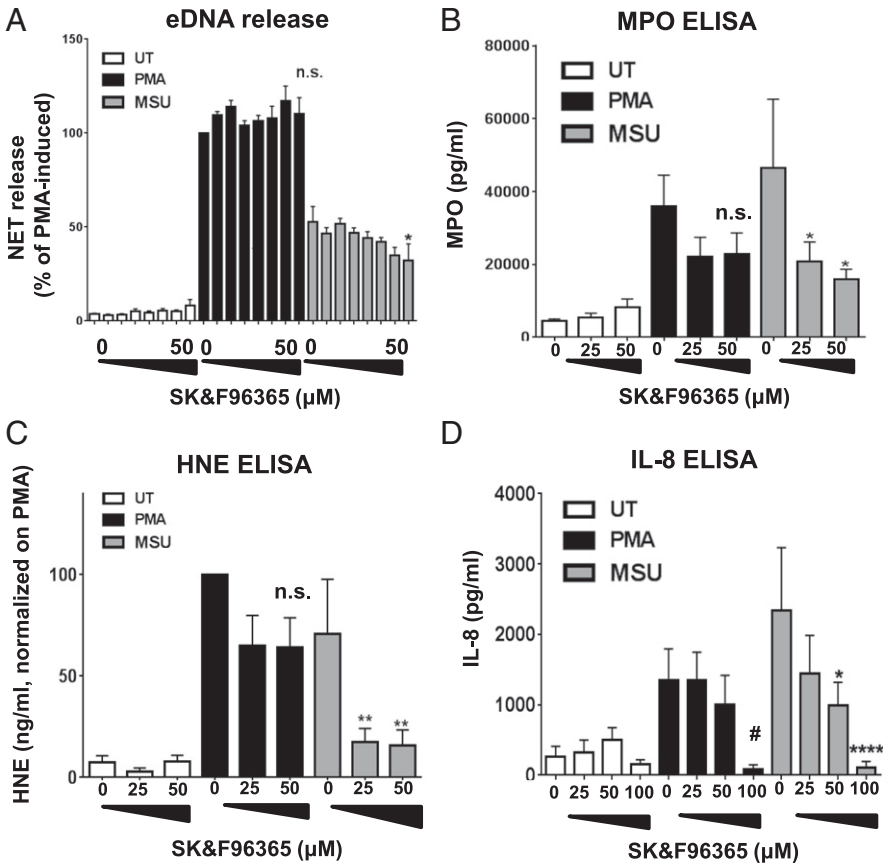

FIGURE 9. The SOCE pathway contributes to PMN activation by MSU crystals. Human PMNs were treated with the SOCE inhibitor SK&F96365 for 45 min prior to stimulation with 250 μg/ml MSU crystals or 100 nM PMA for 3 h. SK&F96365 has significantly reduced (**A**) extracellular DNA (eDNA) release ($n = 5$, mean ± SEM), (**B**) MPO release ($n = 6$, mean ± SEM), (**C**) HNE release ($n = 5$, mean ± SEM), and (**D**) IL-8 secretion ($n = 4$, mean ± SEM) induced by MSU crystals but not by PMA (mean ± SEM, $n = 4$). $^{*}p < 0.05$, $^{**}p < 0.01$, $^{****}p < 0.0001$, $^{\#}p < 0.05$, Dunnett MCT. UT, untreated (no PMA or MSU).

species production, and NET release suggest its promising clinical potential to prevent or attenuate PMN-mediated gouty inflammation. MRS2578 has already been used in a few mouse studies and proved to be nontoxic in a concentration range also used in the present study (107, 110, 111). Future animal studies are required to test its usefulness to treat gout.

P2Y6R is a G protein–coupled receptor and signals via intracellular calcium (112). P2Y6R activates phospholipase Cγ, produces inositol 1,4,5-triphosphate, and activates inositol 1,4,5-triphosphate receptors in the endoplasmic reticulum (ER) (59), resulting in an abrupt spike in cytosolic calcium levels. Depletion of ER calcium stores leads to the activation of the SOCE mechanism (113). STIM1 works as a sensor of ER luminal calcium and redistributes to the ER luminal position to Orai1 spanning the plasma membrane (84, 114). STIM1$^{-/-}$, STIM2$^{-/-}$, and Orai$^{-/-}$ microglial cells do not perform P2Y6R-mediated phagocytosis (115). SOCE is the main mechanism of calcium signaling in PMNs during activation (113). SOCE is mediated by STIM1 and Orai1 proteins (59). Recent studies proposed that the SOCE is required for optimal respiratory burst in PMNs because Stim1-deficient murine PMNs are impaired in superoxide production (116). This suggests that reduction of NET formation by the SOCE inhibitor is caused by diminished NADPH oxidase activity.

Based on our data, we propose that P2Y6R activates SOCE signaling that mediates IL-8–dependent migration of PMNs (35, 86). IL-8 has two receptors, CXCR1 and CXCR2, both of which are expressed on PMNs (117–119). Future investigations are needed to decide which one of these receptors is a major contributor to aggNET formation. Additionally, cytosolic calcium mediated by SOCE could also promote NET formation by activating PAD4, a calcium-dependent enzyme essential for NET release (120). PAD4 citrullinates histone H3 and H4 and promotes chromatin decondensation (121). Although SK&F96365 inhibits SOCE in PMNs (89), inhibition of other calcium channels by this compound has also been reported (122). Studies using Stim1- or Ora1-deficient murine PMNs would further clarify the exact mechanism (116).

NETs represent a double-edged sword because they can either drive or resolve inflammation (6). During the acute phase of gout, PMNs encounter MSU crystals to form NETs and release proinflammatory cytokines (6, 102). When MSU crystal–triggered NETs reach a certain threshold and start forming aggNETs, they cleave proinflammatory cytokines and create a synovial environment more conducive to healing (6, 25). Gouty tophi are formed at this stage. In fact, aggNETs have been proposed to be the core structural unit of tophi (6). This phenomenon seems to be unique to gout.

We used high-throughput confocal imaging to record real-time NET formation. This novel methodology enables us not only to measure NET formation but also PMN migration. It provides us the unique opportunity to understand MSU crystal–PMN and PMN–PMN interactions. Our hypothesis (active migration of PMNs is essential to form aggNETs) suggests a novel "social networking" component among PMNs.

In summary, our work proposes that P2Y6R-mediated purinergic signaling is a crucial component of MSU crystal–induced aggNET formation and gout pathogenesis. It also suggests that targeting P2Y6R offers a novel approach to interfere with acute inflammation in gout.

Acknowledgments

We thank the personnel at the University of Georgia University Health Center for blood collection, and the College of Veterinary Medicine Imaging Core facility for assistance with confocal microscopy and flow cytometry. We are thankful to all of the volunteers who donated blood for our research study. We are grateful to Donald L. Evans (University of Georgia) for scientific input on purinergic receptors.

Disclosures

The authors have no financial conflicts of interest.

References

1. Kuo, C. F., M. J. Grainge, W. Zhang, and M. Doherty. 2015. Global epidemiology of gout: prevalence, incidence and risk factors. *Nat. Rev. Rheumatol.* 11: 649–662.
2. Abbott, K. C., P. L. Kimmel, V. Dharnidharka, R. J. Oglesby, L. Y. Agodoa, and S. Caillard. 2005. New-onset gout after kidney transplantation: incidence, risk factors and implications. *Transplantation* 80: 1383–1391.
3. Abbott, R. D., F. N. Brand, W. B. Kannel, and W. P. Castelli. 1988. Gout and coronary heart disease: the Framingham Study. *J. Clin. Epidemiol.* 41: 237–242.
4. Ask-Upmark, E., and L. Adner. 1951. Coronary infarction and gout. *Acta Med. Scand.* 139: 1–6.
5. Roddy, E., and M. Doherty. 2010. Epidemiology of gout. *Arthritis Res. Ther.* 12: 223.
6. Schauer, C., C. Janko, L. E. Munoz, Y. Zhao, D. Kienhöfer, B. Frey, M. Lell, B. Manger, J. Rech, E. Naschberger, et al. 2014. Aggregated neutrophil extracellular traps limit inflammation by degrading cytokines and chemokines. *Nat. Med.* 20: 511–517.
7. Mitroulis, I., K. Kambas, A. Chrysanthopoulou, P. Skendros, E. Apostolidou, I. Kourtzelis, G. I. Drosos, D. T. Boumpas, and K. Ritis. 2011. Neutrophil extracellular trap formation is associated with IL-1β and autophagy-related signaling in gout. *PLoS One* 6: e29318.
8. Mitroulis, I., K. Kambas, and K. Ritis. 2013. Neutrophils, IL-1β, and gout: is there a link? *Semin. Immunopathol.* 35: 501–512.
9. So, A. 2007. [Recent advances in the pathophysiology of hyperuricemia and gout]. *Rev. Med. Suisse* 3: 720–, 722–724.
10. So, A. 2010. Epidemiology: gout—bad for the heart as well as the joint. *Nat. Rev. Rheumatol.* 6: 386–387.
11. So, A. 2013. How to regulate neutrophils in gout. *Arthritis Res. Ther.* 15: 118.
12. So, A., and N. Busso. 2009. A magic bullet for gout? *Ann. Rheum. Dis.* 68: 1517–1519.
13. So, A. 2008. Developments in the scientific and clinical understanding of gout. *Arthritis Res. Ther.* 10: 221.
14. Busso, N., and H. K. Ea. 2012. The mechanisms of inflammation in gout and pseudogout (CPP-induced arthritis). *Reumatismo* 63: 230–237.
15. Martinon, F., V. Pétrilli, A. Mayor, A. Tardivel, and J. Tschopp. 2006. Gout-associated uric acid crystals activate the NALP3 inflammasome. *Nature* 440: 237–241.
16. Pétrilli, V., and F. Martinon. 2007. The inflammasome, autoinflammatory diseases, and gout. *Joint Bone Spine* 74: 571–576.
17. Oliveira, S. H., C. Canetti, R. A. Ribeiro, and F. Q. Cunha. 2008. Neutrophil migration induced by IL-1β depends upon LTB4 released by macrophages and upon TNF-α and IL-1β released by mast cells. *Inflammation* 31: 36–46.
18. Brinkmann, V., and A. Zychlinsky. 2007. Beneficial suicide: why neutrophils die to make NETs. *Nat. Rev. Microbiol.* 5: 577–582.
19. Brinkmann, V., and A. Zychlinsky. 2012. Neutrophil extracellular traps: is immunity the second function of chromatin? *J. Cell Biol.* 198: 773–783.
20. Brinkmann, V., U. Reichard, C. Goosmann, B. Fauler, Y. Uhlemann, D. S. Weiss, Y. Weinrauch, and A. Zychlinsky. 2004. Neutrophil extracellular traps kill bacteria. *Science* 303: 1532–1535.
21. Fuchs, T. A., U. Abed, C. Goosmann, R. Hurwitz, I. Schulze, V. Wahn, Y. Weinrauch, V. Brinkmann, and A. Zychlinsky. 2007. Novel cell death program leads to neutrophil extracellular traps. *J. Cell Biol.* 176: 231–241.
22. Grayson, P. C., and M. J. Kaplan. 2016. At the Bench: neutrophil extracellular traps (NETs) highlight novel aspects of innate immune system involvement in autoimmune diseases. *J. Leukoc. Biol.* 99: 253–264.
23. Stoiber, W., A. Obermayer, P. Steinbacher, and W. D. Krautgartner. 2015. The role of reactive oxygen species (ROS) in the formation of extracellular traps (ETs) in humans. *Biomolecules* 5: 702–723.
24. Wang, J., and H. Arase. 2014. Regulation of immune responses by neutrophils. *Ann. N. Y. Acad. Sci.* 1319: 66–81.
25. Christine Czegley, M. B., D. Weidner, M. Hoffmann, M. Herrmann, and C. Schauer. 2014. Monocytes and granulocytes orchestrate induction and resolution of inflammation in gout. *Gout Hyperuricemia* 1: 88–93.
26. Chhana, A., and N. Dalbeth. 2015. The gouty tophus: a review. *Curr. Rheumatol. Rep.* 17: 19.
27. Desai, J., S. V. Kumar, S. R. Mulay, L. Konrad, S. Romoli, C. Schauer, M. Herrmann, R. Bilyy, S. Müller, B. Popper, et al. 2016. PMA and crystal-induced neutrophil extracellular trap formation involves RIPK1-RIPK3-MLKL signaling. *Eur. J. Immunol.* 46: 223–229.
28. Uratsuji, H., Y. Tada, T. Kawashima, M. Kamata, C. S. Hau, Y. Asano, M. Sugaya, T. Kadono, A. Asahina, S. Sato, and K. Tamaki. 2012. $P2Y_6$ receptor signaling pathway mediates inflammatory responses induced by monosodium urate crystals. *J. Immunol.* 188: 436–444.
29. Abbracchio, M. P., G. Burnstock, J. M. Boeynaems, E. A. Barnard, J. L. Boyer, C. Kennedy, G. E. Knight, M. Fumagalli, C. Gachet, K. A. Jacobson, and G. A. Weisman. 2006. International Union of Pharmacology LVIII: update on the P2Y G protein-coupled nucleotide receptors: from molecular mechanisms and pathophysiology to therapy. *Pharmacol. Rev.* 58: 281–341.
30. von Kugelgen, I., and K. Hoffmann. 2016. Pharmacology and structure of P2Y receptors. *Neuropharmacology.* 50–61.
31. Junger, W. G. 2011. Immune cell regulation by autocrine purinergic signalling. *Nat. Rev. Immunol.* 11: 201–212.
32. Taylor, W. J., H. R. Schumacher, Jr., H. S. Baraf, P. Chapman, L. Stamp, M. Doherty, F. McQueen, N. Dalbeth, N. Schlesinger, D. E. Furst, et al. 2008. A modified Delphi exercise to determine the extent of consensus with OMERACT outcome domains for studies of acute and chronic gout. [Published erratum appears in 2006 *Ann. Rheum. Dis.* 67: 1652.] *Ann. Rheum. Dis.* 67: 888–891.
33. Grassi, F. 2010. Purinergic control of neutrophil activation. *J. Mol. Cell Biol.* 2: 176–177.
34. Hidalgo, M. A., M. D. Carretta, S. E. Teuber, C. Zárate, L. Cárcamo, I. I. Concha, and R. A. Burgos. 2015. fMLP-induced IL-8 release is dependent on NADPH oxidase in human neutrophils. *J. Immunol. Res.* 2015: 120348.
35. Campwala, H., D. W. Sexton, D. C. Crossman, and S. J. Fountain. 2014. $P2Y_6$ receptor inhibition perturbs CCL2-evoked signalling in human monocytic and peripheral blood mononuclear cells. *J. Cell Sci.* 127: 4964–4973.
36. Grbic, D. M., E. Degagné, C. Langlois, A. A. Dupuis, and F. P. Gendron. 2008. Intestinal inflammation increases the expression of the $P2Y_6$ receptor on epithelial cells and the release of CXC chemokine ligand 8 by UDP. *J. Immunol.* 180: 2659–2668.
37. Khine, A. A., L. Del Sorbo, R. Vaschetto, S. Voglis, E. Tullis, A. S. Slutsky, G. P. Downey, and H. Zhang. 2006. Human neutrophil peptides induce interleukin-8 production through the $P2Y_6$ signaling pathway. *Blood* 107: 2936–2942.
38. Xiang, Z., and G. Burnstock. 2006. Distribution of $P2Y_6$ and $P2Y_{12}$ receptor: their colocalization with calbindin, calretinin and nitric oxide synthase in the guinea pig enteric nervous system. *Histochem. Cell Biol.* 125: 327–336.
39. Schreiber, R., and K. Kunzelmann. 2005. Purinergic $P2Y_6$ receptors induce Ca^{2+} and CFTR dependent Cl^- secretion in mouse trachea. *Cell. Physiol. Biochem.* 16: 99–108.
40. Cox, M. A., B. Gomes, K. Palmer, K. Du, M. Wiekowski, B. Wilburn, M. Petro, C. C. Chou, C. Desquitado, M. Schwarz, et al. 2005. The pyrimidinergic $P2Y_6$ receptor mediates a novel release of proinflammatory cytokines and chemokines in monocytic cells stimulated with UDP. *Biochem. Biophys. Res. Commun.* 330: 467–473.
41. Korcok, J., L. N. Raimundo, X. Du, S. M. Sims, and S. J. Dixon. 2005. P2Y6 nucleotide receptors activate NF-κB and increase survival of osteoclasts. *J. Biol. Chem.* 280: 16909–16915.
42. Hansen, A., L. Alston, S. E. Tulk, L. P. Schenck, M. E. Grassie, B. F. Alhassan, A. T. Veermalla, S. Al-Bashir, F. P. Gendron, C. Altier, et al. 2013. The $P2Y_6$ receptor mediates *Clostridium difficile* toxin-induced CXCL8/IL-8 production and intestinal epithelial barrier dysfunction. *PLoS One* 8: e81491.
43. Liu, G. D., J. Q. Ding, Q. Xiao, and S. D. Chen. 2009. P2Y6 receptor and immunoinflammation. *Neurosci. Bull.* 25: 161–164.
44. Yoo, D. G., M. Floyd, M. Winn, S. M. Moskowitz, and B. Rada. 2014. NET formation induced by *Pseudomonas aeruginosa* cystic fibrosis isolates measured as release of myeloperoxidase–DNA and neutrophil elastase–DNA complexes. *Immunol. Lett.* 160: 186–194.
45. Yoo, D. G., M. Winn, L. Pang, S. M. Moskowitz, H. L. Malech, T. L. Leto, and B. Rada. 2014. Release of cystic fibrosis airway inflammatory markers from *Pseudomonas aeruginosa*–stimulated human neutrophils involves NADPH oxidase-dependent extracellular DNA trap formation. *J. Immunol.* 192: 4728–4738.
46. Altman, R., E. Asch, D. Bloch, G. Bole, D. Borenstein, K. Brandt, W. Christy, T. D. Cooke, R. Greenwald, M. Hochberg, et al; Diagnostic and Therapeutic Criteria Committee of the American Rheumatism Association. 1986. Development of criteria for the classification and reporting of osteoarthritis. Classification of osteoarthritis of the knee. *Arthritis Rheum.* 29: 1039–1049.
47. Pang, L., C. P. Hayes, K. Buac, D. G. Yoo, and B. Rada. 2013. Pseudogout-associated inflammatory calcium pyrophosphate dihydrate microcrystals induce formation of neutrophil extracellular traps. *J. Immunol.* 190: 6488–6500.
48. Sil, P., D. G. Yoo, M. Floyd, A. Gingerich, and B. Rada. 2016. High throughput measurement of extracellular DNA release and quantitative NET formation in human neutrophils in vitro. *J. Vis. Exp.* 112: e52779. Available at: https://www.jove.com/video/52779/high-throughput-measurement-extracellular-dna-release-quantitative.
49. Watford, W. T., D. Li, D. Agnello, L. Durant, K. Yamaoka, Z. J. Yao, H. J. Ahn, T. P. Cheng, S. R. Hofmann, T. Cogliati, et al. 2006. Cytohesin binder and regulator (Cybr) is not essential for T- and dendritic-cell activation and differentiation. *Mol. Cell. Biol.* 26: 6623–6632.
50. Zhang, E., X. Yan, M. Zhang, X. Chang, Z. Bai, Y. He, and Z. Yuan. 2013. Aggrecanases in the human synovial fluid at different stages of osteoarthritis. *Clin. Rheumatol.* 32: 797–803.
51. Robinson, W. H., C. M. Lepus, Q. Wang, H. Raghu, R. Mao, T. M. Lindstrom, and J. Sokolove. 2016. Low-grade inflammation as a key mediator of the pathogenesis of osteoarthritis. *Nat. Rev. Rheumatol.* 12: 580–592.
52. Popa-Nita, O., and P. H. Naccache. 2010. Crystal-induced neutrophil activation. *Immunol. Cell Biol.* 88: 32–40.
53. Busso, N., and A. So. 2010. Mechanisms of inflammation in gout. *Arthritis Res. Ther.* 12: 206.
54. Carulli, G., A. Marini, A. Azzarà, M. Petrini, L. Ruocco, and F. Ambrogi. 1985. Modifications in the phagocytosis of human neutrophils induced by vinblastine and cytochalasin B: the effects of lithium. *Acta Haematol.* 74: 81–85.
55. Chen, Y., Y. Yao, Y. Sumi, A. Li, U. K. To, A. Elkhal, Y. Inoue, T. Woehrle, Q. Zhang, C. Hauser, and W. G. Junger. 2010. Purinergic signaling: a fundamental mechanism in neutrophil activation. *Sci. Signal.* 3: ra45.
56. Laubinger, W., H. Wang, T. Welte, and G. Reiser. 2003. P2Y receptor specific for diadenosine tetraphosphate in lung: selective inhibition by suramin, PPADS, Ip5I, and not by MRS-2197. *Eur. J. Pharmacol.* 468: 9–14.

57. Charlton, S. J., C. A. Brown, G. A. Weisman, J. T. Turner, L. Erb, and M. R. Boarder. 1996. PPADS and suramin as antagonists at cloned P2Y- and P2U-purinoceptors. *Br. J. Pharmacol.* 118: 704–710.
58. Usune, S., T. Katsuragi, and T. Furukawa. 1996. Effects of PPADS and suramin on contractions and cytoplasmic Ca^{2+} changes evoked by AP_4A, ATP and α,β-methylene ATP in guinea-pig urinary bladder. *Br. J. Pharmacol.* 117: 698–702.
59. Lewis, R. S. 2011. Store-operated calcium channels: new perspectives on mechanism and function. *Cold Spring Harb. Perspect. Biol.* 3: a003970. Available at: http://cshperspectives.cshlp.org/content/3/12/a003970.full.
60. Braganhol, E., F. Kukulski, S. A. Lévesque, M. Fausther, E. G. Lavoie, A. Zanotto-Filho, L. S. Bergamin, J. Pelletier, F. Bahrami, F. Ben Yebdri, et al. 2015. Nucleotide receptors control IL-8/CXCL8 and MCP-1/CCL2 secretions as well as proliferation in human glioma cells. *Biochim. Biophys. Acta* 1852: 120–130.
61. Mély, Y., M. Cadène, I. Sylte, and J. G. Bieth. 1997. Mapping the suramin-binding sites of human neutrophil elastase: investigation by fluorescence resonance energy transfer and molecular modeling. *Biochemistry* 36: 15624–15631.
62. Cadène, M., J. Duranton, A. North, M. Si-Tahar, M. Chignard, and J. G. Bieth. 1997. Inhibition of neutrophil serine proteinases by suramin. *J. Biol. Chem.* 272: 9950–9955.
63. Metzler, K. D., C. Goosmann, A. Lubojemska, A. Zychlinsky, and V. Papayannopoulos. 2014. A myeloperoxidase-containing complex regulates neutrophil elastase release and actin dynamics during NETosis. *Cell Rep.* 8: 883–896.
64. Papayannopoulos, V., K. D. Metzler, A. Hakkim, and A. Zychlinsky. 2010. Neutrophil elastase and myeloperoxidase regulate the formation of neutrophil extracellular traps. *J. Cell Biol.* 191: 677–691.
65. Martinod, K., T. Witsch, K. Farley, M. Gallant, E. Remold-O'Donnell, and D. D. Wagner. 2016. Neutrophil elastase-deficient mice form neutrophil extracellular traps in an experimental model of deep vein thrombosis. *J. Thromb. Haemost.* 14: 551–558.
66. Crocetti, L., I. A. Schepetkin, A. Cilibrizzi, A. Graziano, C. Vergelli, D. Giomi, A. I. Khlebnikov, M. T. Quinn, and M. P. Giovannoni. 2013. Optimization of *N*-benzoylindazole derivatives as inhibitors of human neutrophil elastase. *J. Med. Chem.* 56: 6259–6272.
67. El-Tayeb, A., A. Qi, and C. E. Müller. 2006. Synthesis and structure–activity relationships of uracil nucleotide derivatives and analogues as agonists at human $P2Y_2$, $P2Y_4$, and $P2Y_6$ receptors. *J. Med. Chem.* 49: 7076–7087.
68. Ko, H., R. L. Carter, L. Cosyn, R. Petrelli, S. de Castro, P. Besada, Y. Zhou, L. Cappellacci, P. Franchetti, M. Grifantini, et al. 2008. Synthesis and potency of novel uracil nucleotides and derivatives as $P2Y_2$ and $P2Y_6$ receptor agonists. *Bioorg. Med. Chem.* 16: 6319–6332.
69. Önnheim, K., K. Christenson, M. Gabl, J. C. Burbiel, C. E. Müller, T. I. Oprea, J. Bylund, C. Dahlgren, and H. Forsman. 2014. A novel receptor cross-talk between the ATP receptor $P2Y_2$ and formyl peptide receptors reactivates desensitized neutrophils to produce superoxide. *Exp. Cell Res.* 323: 209–217.
70. Jacob, F., C. Pérez Novo, C. Bachert, and K. Van Crombruggen. 2013. Purinergic signaling in inflammatory cells: P2 receptor expression, functional effects, and modulation of inflammatory responses. *Purinergic Signal.* 9: 285–306.
71. Mamedova, L. K., B. V. Joshi, Z. G. Gao, I. von Kügelgen, and K. A. Jacobson. 2004. Diisothiocyanate derivatives as potent, insurmountable antagonists of $P2Y_6$ nucleotide receptors. *Biochem. Pharmacol.* 67: 1763–1770.
72. Nagaoka, I., K. Suzuki, T. Murakami, F. Niyonsaba, H. Tamura, and M. Hirata. 2010. Evaluation of the effect of α-defensin human neutrophil peptides on neutrophil apoptosis. *Int. J. Mol. Med.* 26: 925–934.
73. Yu, W., and W. G. Hill. 2013. Lack of specificity shown by $P2Y_6$ receptor antibodies. *Naunyn Schmiedebergs Arch. Pharmacol.* 386: 885–891.
74. Cekic, C., and J. Linden. 2016. Purinergic regulation of the immune system. *Nat. Rev. Immunol.* 16: 177–192.
75. Chen, J., Y. Zhao, and Y. Liu. 2014. The role of nucleotides and purinergic signaling in apoptotic cell clearance—implications for chronic inflammatory diseases. *Front. Immunol.* 5: 656.
76. Ginsburg-Shmuel, T., M. Haas, D. Grbic, G. Arguin, Y. Nadel, F. P. Gendron, G. Reiser, and B. Fischer. 2012. UDP made a highly promising stable, potent, and selective P2Y6-receptor agonist upon introduction of a boranophosphate moiety. *Bioorg. Med. Chem.* 20: 5483–5495.
77. Koizumi, S., Y. Shigemoto-Mogami, K. Nasu-Tada, Y. Shinozaki, K. Ohsawa, M. Tsuda, B. V. Joshi, K. A. Jacobson, S. Kohsaka, and K. Inoue. 2007. UDP acting at $P2Y_6$ receptors is a mediator of microglial phagocytosis. *Nature* 446: 1091–1095.
78. Neher, J. J., U. Neniskyte, T. Hornik, and G. C. Brown. 2014. Inhibition of UDP/$P2Y_6$ purinergic signaling prevents phagocytosis of viable neurons by activated microglia in vitro and in vivo. *Glia* 62: 1463–1475.
79. Keshari, R. S., A. Jyoti, M. Dubey, N. Kothari, M. Kohli, J. Bogra, M. K. Barthwal, and M. Dikshit. 2012. Cytokines induced neutrophil extracellular traps formation: implication for the inflammatory disease condition. *PLoS One* 7: e48111.
80. Hazeldine, J., P. Harris, I. L. Chapple, M. Grant, H. Greenwood, A. Livesey, E. Sapey, and J. M. Lord. 2014. Impaired neutrophil extracellular trap formation: a novel defect in the innate immune system of aged individuals. *Aging Cell* 13: 690–698.
81. Rada, B. K., M. Geiszt, K. Káldi, C. Timár, and E. Ligeti. 2004. Dual role of phagocytic NADPH oxidase in bacterial killing. *Blood* 104: 2947–2953.
82. Rada, B., M. A. Jendrysik, L. Pang, C. P. Hayes, D. G. Yoo, J. J. Park, S. M. Moskowitz, H. L. Malech, and T. L. Leto. 2013. Pyocyanin-enhanced neutrophil extracellular trap formation requires the NADPH oxidase. *PLoS One* 8: e54205.
83. Zizzo, M. G., M. Mastropaolo, J. Grählert, F. Mulè, and R. Serio. 2012. Pharmacological characterization of uracil nucleotide-preferring P2Y receptors modulating intestinal motility: a study on mouse ileum. *Purinergic Signal.* 8: 275–285.
84. Douda, D. N., M. A. Khan, H. Grasemann, and N. Palaniyar. 2015. SK3 channel and mitochondrial ROS mediate NADPH oxidase-independent NETosis induced by calcium influx. *Proc. Natl. Acad. Sci. USA* 112: 2817–2822.
85. Grbic, D. M., É. Degagné, J. F. Larrivée, M. S. Bilodeau, V. Vinette, G. Arguin, J. Stankova, and F. P. Gendron. 2012. P2Y6 receptor contributes to neutrophil recruitment to inflamed intestinal mucosa by increasing CXC chemokine ligand 8 expression in an AP-1-dependent manner in epithelial cells. *Inflamm. Bowel Dis.* 18: 1456–1469.
86. Ide, S., N. Nishimaki, M. Tsukimoto, and S. Kojima. 2014. Purine receptor $P2Y_6$ mediates cellular response to γ-ray-induced DNA damage. *J. Toxicol. Sci.* 39: 15–23.
87. Inoue, K. 2007. UDP facilitates microglial phagocytosis through P2Y6 receptors. *Cell Adhes. Migr.* 1: 131–132.
88. Rada, B. K., M. Geiszt, R. Van Bruggen, K. Nemet, D. Roos, and E. Ligeti. 2003. Calcium signalling is altered in myeloid cells with a deficiency in NADPH oxidase activity. *Clin. Exp. Immunol.* 132: 53–60.
89. Clemens, R. A., and C. A. Lowell. 2015. Store-operated calcium signaling in neutrophils. *J. Leukoc. Biol.* 98: 497–502.
90. Travis, J. 1988. Structure, function, and control of neutrophil proteinases. *Am. J. Med.* 84(6A): 37–42.
91. Watorek, W., D. Farley, G. Salvesen, and J. Travis. 1988. Neutrophil elastase and cathepsin G: structure, function, and biological control. *Adv. Exp. Med. Biol.* 240: 23–31.
92. Amitani, R., R. Wilson, A. Rutman, R. Read, C. Ward, D. Burnett, R. A. Stockley, and P. J. Cole. 1991. Effects of human neutrophil elastase and *Pseudomonas aeruginosa* proteinases on human respiratory epithelium. *Am. J. Respir. Cell Mol. Biol.* 4: 26–32.
93. Lucey, E. C., P. J. Stone, R. Breuer, T. G. Christensen, J. D. Calore, A. Catanese, C. Franzblau, and G. L. Snider. 1985. Effect of combined human neutrophil cathepsin G and elastase on induction of secretory cell metaplasia and emphysema in hamsters, with in vitro observations on elastolysis by these enzymes. *Am. Rev. Respir. Dis.* 132: 362–366.
94. Smallman, L. A., S. L. Hill, and R. A. Stockley. 1984. Reduction of ciliary beat frequency in vitro by sputum from patients with bronchiectasis: a serine proteinase effect. *Thorax* 39: 663–667.
95. Sly, P. D., C. L. Gangell, L. Chen, R. S. Ware, S. Ranganathan, L. S. Mott, C. P. Murray, and S. M. Stick, AREST CF Investigators. 2013. Risk factors for bronchiectasis in children with cystic fibrosis. *N. Engl. J. Med.* 368: 1963–1970.
96. Hoenderdos, K., and A. Condliffe. 2013. The neutrophil in chronic obstructive pulmonary disease. *Am. J. Respir. Cell Mol. Biol.* 48: 531–539.
97. Sandhaus, R. A., and G. Turino. 2013. Neutrophil elastase-mediated lung disease. *COPD* 10(Suppl 1): 60–63.
98. Neogi, T., T. L. Jansen, N. Dalbeth, J. Fransen, H. R. Schumacher, D. Berendsen, M. Brown, H. Choi, N. L. Edwards, H. J. Janssens, et al. 2015. 2015 Gout classification criteria: an American College of Rheumatology/European League against Rheumatism collaborative initiative. [Published erratum appears in 2016 *Ann. Rheum. Dis.* 75: 473.] *Ann. Rheum. Dis.* 74: 1789–1798.
99. Ogdie, A., W. J. Taylor, M. Weatherall, J. Fransen, T. L. Jansen, T. Neogi, H. R. Schumacher, and N. Dalbeth. 2015. Imaging modalities for the classification of gout: systematic literature review and meta-analysis. *Ann. Rheum. Dis.* 74: 1868–1874.
100. Taylor, W. J., J. Fransen, T. L. Jansen, N. Dalbeth, H. R. Schumacher, M. Brown, W. Louthrenoo, J. Vazquez-Mellado, M. Eliseev, G. McCarthy, et al. 2015. Study for updated gout classification criteria: identification of features to classify gout. *Arthritis Care Res. (Hoboken)* 67: 1304–1315.
101. Schorn, C., C. Janko, M. Latzko, R. Chaurio, G. Schett, and M. Herrmann. 2012. Monosodium urate crystals induce extracellular DNA traps in neutrophils, eosinophils, and basophils but not in mononuclear cells. *Front. Immunol.* 3: 277.
102. Dalbeth, N., T. R. Merriman, and L. K. Stamp. 2016. Gout. *Lancet* 388: 2039–2052.
103. Arai, Y., Y. Nishinaka, T. Arai, M. Morita, K. Mizugishi, S. Adachi, A. Takaori-Kondo, T. Watanabe, and K. Yamashita. 2013. Uric acid induces NADPH oxidase-independent neutrophil extracellular trap formation. *Biochem. Biophys. Res. Commun.*
104. Dahl, G. 2015. ATP release through pannexon channels. *Philos. Trans. R. Soc. Lond. B Biol. Sci.* 370: 370.
105. Hoyle, C. H., G. E. Knight, and G. Burnstock. 1990. Suramin antagonizes responses to P2-purinoceptor agonists and purinergic nerve stimulation in the guinea-pig urinary bladder and taenia coli. *Br. J. Pharmacol.* 99: 617–621.
106. Ralevic, V., and G. Burnstock. 1996. Discrimination by PPADS between endothelial P2Y- and P2U-purinoceptors in the rat isolated mesenteric arterial bed. *Br. J. Pharmacol.* 118: 428–434.
107. Li, R., B. Tan, Y. Yan, X. Ma, N. Zhang, Z. Zhang, M. Liu, M. Qian, and B. Du. 2014. Extracellular UDP and $P2Y_6$ function as a danger signal to protect mice from vesicular stomatitis virus infection through an increase in IFN-β production. *J. Immunol.* 193: 4515–4526.
108. Kukulski, F., F. Ben Yebdri, J. Lefebvre, M. Warny, P. A. Tessier, and J. Sévigny. 2007. Extracellular nucleotides mediate LPS-induced neutrophil migration in vitro and in vivo. *J. Leukoc. Biol.* 81: 1269–1275.
109. Ibusuki, K., T. Sakiyama, S. Kanmura, T. Maeda, Y. Iwashita, Y. Nasu, F. Sasaki, H. Taguchi, S. Hashimoto, M. Numata, et al. 2015. Human neutrophil peptides induce interleukin-8 in intestinal epithelial cells through the P2 receptor and ERK1/2 signaling pathways. *Int. J. Mol. Med.* 35: 1603–1609.

110. Syhr, K. M., W. Kallenborn-Gerhardt, R. Lu, K. Olbrich, K. Schmitz, J. Männich, N. Ferreiros-Bouzas, G. Geisslinger, E. Niederberger, and A. Schmidtko. 2014. Lack of effect of a P2Y6 receptor antagonist on neuropathic pain behavior in mice. *Pharmacol. Biochem. Behav.* 124: 389–395.
111. Zhang, Z., Z. Wang, H. Ren, M. Yue, K. Huang, H. Gu, M. Liu, B. Du, and M. Qian. 2011. $P2Y_6$ agonist uridine 5′-diphosphate promotes host defense against bacterial infection via monocyte chemoattractant protein-1-mediated monocytes/macrophages recruitment. *J. Immunol.* 186: 5376–5387.
112. Itagaki, K., K. B. Kannan, D. H. Livingston, E. A. Deitch, Z. Fekete, and C. J. Hauser. 2002. Store-operated calcium entry in human neutrophils reflects multiple contributions from independently regulated pathways. *J. Immunol.* 168: 4063–4069.
113. Demaurex, N., and P. Nunes. 2016. The role of STIM and ORAI proteins in phagocytic immune cells. *Am. J. Physiol. Cell. Physiol.* 310: C496–C508.
114. Dixit, N., and S. I. Simon. 2012. Chemokines, selectins and intracellular calcium flux: temporal and spatial cues for leukocyte arrest. *Front. Immunol.* 3: 188.
115. Michaelis, M., B. Nieswandt, D. Stegner, J. Eilers, and R. Kraft. 2015. STIM1, STIM2, and Orai1 regulate store-operated calcium entry and purinergic activation of microglia. *Glia* 63: 652–663.
116. Zhang, H., R. A. Clemens, F. Liu, Y. Hu, Y. Baba, P. Theodore, T. Kurosaki, and C. A. Lowell. 2014. STIM1 calcium sensor is required for activation of the phagocyte oxidase during inflammation and host defense. *Blood* 123: 2238–2249.
117. Almasi, S., M. R. Aliparasti, M. Farhoudi, Z. Babaloo, B. Baradaran, F. Zamani, H. Sadeghi-Bazargani, S. Mostafaei, and E. S. Hokmabadi. 2013. Quantitative evaluation of CXCL8 and its receptors (CXCR1 and CXCR2) gene expression in Iranian patients with multiple sclerosis. *Immunol. Invest.* 42: 737–748.
118. Reyes-Robles, T., F. Alonzo, III, L. Kozhaya, D. B. Lacy, D. Unutmaz, and V. J. Torres. 2013. *Staphylococcus aureus* leukotoxin ED targets the chemokine receptors CXCR1 and CXCR2 to kill leukocytes and promote infection. *Cell Host Microbe* 14: 453–459.
119. Alonzo III, F., L. Kozhaya, S. A. Rawlings, T. Reyes-Robles, A. L. DuMont, D. G. Myszka, N. R. Landau, D. Unutmaz, and V. J. Torres. 2013. CCR5 is a receptor for *Staphylococcus aureus* leukotoxin ED. *Nature* 493: 51–55.
120. Jones, J. E., C. P. Causey, B. Knuckley, J. L. Slack-Noyes, and P. R. Thompson. 2009. Protein arginine deiminase 4 (PAD4): current understanding and future therapeutic potential. *Curr. Opin. Drug Discov. Devel.* 12: 616–627.
121. Gupta, A. K., S. Giaglis, P. Hasler, and S. Hahn. 2014. Efficient neutrophil extracellular trap induction requires mobilization of both intracellular and extracellular calcium pools and is modulated by cyclosporine A. *PLoS One* 9: e97088.
122. Chaïb, N., E. Kabré, M. Métioui, E. Alzola, C. Dantinne, A. Marino, and J. P. Dehaye. 1998. Differential sensitivity to nickel and SK&F96365 of second messenger-operated and receptor-operated calcium channels in rat submandibular ductal cells. *Cell Calcium* 23: 395–404.